12-2010

New Handheld Emissions Detector for Pinpointing the Location of Inadvertently Energized Objects in Urban Environments.

Kermit O. Phipps
East Tennessee State University

New Handheld Emissions Detector for Pinpointing the Location of Inadvertently Energized Objects in Urban Environments

---

A thesis

presented to

the faculty of the Department of Technology

East Tennessee State University

In partial fulfillment

of the requirements for the degree

Master of Science in Technology

---

by

Kermit O. Phipps

December 2010

Dr. W. Andrew Clark, Chair

Dr. J. Paul Sims

Dr. Keith Johnson

Mr. Hugh Broome

Keywords: Handheld detector, emissions, inadvertently energized objects, Order 04-M-0159, mandated city scans, Jodie Lane, pedestrian shocks, animal shocks

ABSTRACT

New Handheld Emissions Detector for Pinpointing the Location of Inadvertently Energized Objects in Urban Environments

by

Kermit O. Phipps

The power distribution infrastructure in the United States is deteriorating at a rapid rate exposing infrastructure wiring and creating potential shock hazards. Periodic road and sidewalk maintenance projects can also expose wiring and create energized objects. In urban settings inadvertently energized objects include: lamp posts, bus shelters, metal street curbs, sign posts, transformer vaults, and manhole covers as well as concrete and asphalt pavement. Every year electric shocks occur when people and domestic animals (such as dogs and cats) make incidental contact with these energized objects. In very rare cases the shocks from these contacts are lethal. Through current personal research, a new handheld detector was developed. It uses the emissions of an energized object to pinpoint the location and further analyzes the emissions to determine the likely cause of the shock hazard. This thesis focuses on advancing detection technology and creating a more capable, production-ready unit.

ACKNOWLEDGEMENTS

I would like to acknowledge my wife Cathy and my son Johnathan for their continued support while I have pursued my education goals. When time for family activities became restricted (which was frequent), I made every attempt to increase the amount of quality family time at the next available opportunity.

I also give my thanks to my parents for their belief that I could overcome my childhood learning and speech disabilities and achieve whatever life goals I set for myself. They never gave me a discouraging word—only their encouragement.

A much deserved thank you to Dr. W. Andrew Clark for standing as my committee chair during the pursuit of my master's degree. I would also like to give a special thanks to Mr. Hugh Broome who reviewed my technical research in depth. In addition, my thanks goes to Dr. Paul Sims for his early suggestions to focus my thesis research on only the handheld unit and to Dr. Keith Johnson for doing me the honor of being a member of my advisory committee.

A grateful thanks to Mr. Doug Dorr, my project manager at Electric Power Research Institute (EPRI), for giving me permission to use my current research for this thesis. Mr. Dorr always believed in me while many others insisted that this project would never be successful.

DEDICATION

This thesis is dedicated to the memory of Jodie Lane.

On January 16, 2004, Jodie Lane was lethally electrocuted by contact voltage on the streets of New York City.

The thesis is also dedicated to Roger Lane, father of Jodie Lane,

for his tireless efforts in alerting the public to the dangers of contact voltages and the need to reduce public shock hazards.

LIST OF TABLES

Table Page

LIST OF FIGURES

Figure Page

CHAPTER 1

INTRODUCTION

This introduction elaborates on the four subsections entitled: New Problem in Urban Electric Infrastructure Recognized, Public Service Commission Mandates City Scans, Results of Mandated City Scans, and Cost of Mandated City Scans.

New Problem in Urban Electric Infrastructure Recognized

Inadvertently energized objects created by breakdowns in the wiring of the electric utility's underground power distribution system have been found to be hazardous to pedestrian traffic and domestic animals (i.e., dogs and cats). In a very limited number of cases these incidental shocks have even proved to be lethal.

New York Public Service Commission Mandates City Scans

After the unfortunate electrocution of Jodie Lane in January 2004, the New York Public Service Commission issued order 04-M-0159 requiring Consolidated Edison to survey all electrical services in its territory and report on the findings and testing proposal. In 2008, in response to public demand for further action, the New York Public Service Commission (PSC) issued a revised order (04-M-0159) requiring:

- Annual testing of all public electrical facilities and street lights.
- Penalties in excess of $200 million for failure to comply with testing requirements
- Twelve mobile scans annually in New York City are required (essentially one scan per month, five days a week, 52 weeks a year to complete 12 city wide scans)
- Upstate cities must be scanned once per year
- Mobile testing of incorporated cities with population > 50,000
- Minimum detection capability of scan equipment must be 6 volts
- Any over-limit contact voltages must be reduced to 1 volt or less
- Annual reporting requirements

Results of Mandated City Scans

The mandated city scan program has been increasingly effective. In 2006 Consolidated Edison, a New York utility, identified 1,214 potential shock hazards (Chan, 2006).

In the next 3 years (2007–2009), the number of energized objects uncovered with the step-upped detection effort increased each year from 1,985 in 2007 to 2,167 in 2008 and then to 3,100 in 2009. Stated otherwise, between January 2007 and December 2009, 7,252 energized objects were found and repaired in Manhattan alone (Foundation, 2010).

Refer to Figure 1 for locations in Manhattan where potential shock hazards have been found. Basically, they were found in all areas of Manhattan. The mainly natural area of Central Park is discernible; refer to Figure 1. Almost no energized objects were uncovered in the park—reflecting a minimal electric infrastructure and a mostly grass and tree setting.

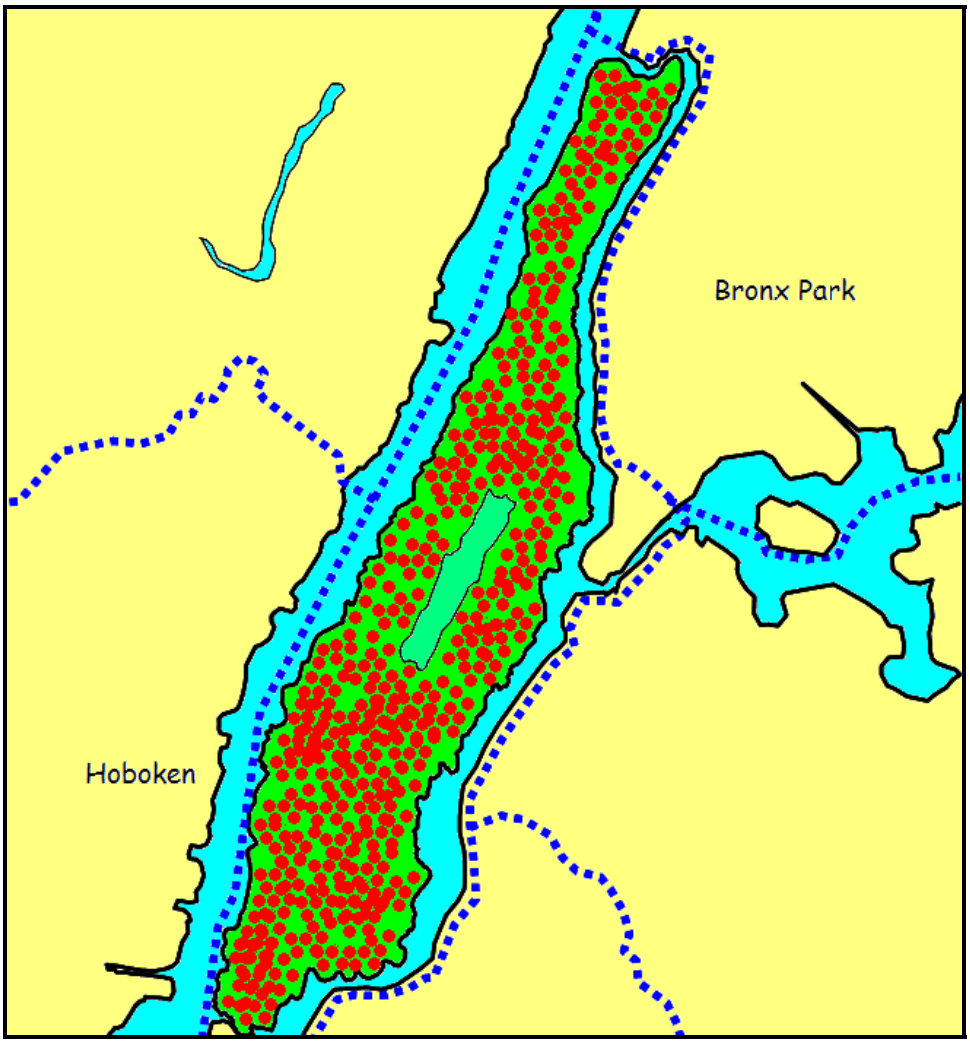

Figure 1. Contact voltage in Manhattan

Costs of Mandated City Scans

Without doubt, the new PSC order has been increasingly effective. However, complying with the new PSC order comes with a cost.

The cost for mobile testing (testing performed by truck-carried detectors) by the three utilities serving the greater New York State area is currently in excess of $11 million annually with manual testing (testing performed by hand measurements) costing in excess of $20 million annually (Hanabuth, 2010).

Projected Savings

As with all expenses, the cost is passed back to the public in rate increases when necessary. Avoiding or reducing rate increases to the consumer is the driver for proposing new technologies to save time and costs.

As an example using the numbers reported by Hanabuth (2010), the estimated cost savings for a contact voltage detector can be estimated using projected variables, such as the number of objects being probed for contact identification and could be projected as follows:

Manual testing costing ConEd 75% of $ 20 million ≈ $ 15 million.
3100 objects detected with 10 objects having been touched = 30,100 objects
Reduction by ½ using the advance handheld detectors,15,050 objects being probed.
Cost of each object ≈ $ 498
$ 498 x 15,050 objects ≈ $ 7.5 million
15 million - $7.5 million
Cost savings of $ 7.5 million

A cost savings of $7.5 million dollars a year is significant and supports the pecuniary implications of using advance identification tools in place of cumbersome probing methods currently being used.

CHAPTER 2

CURRENT DETECTION METHOD

The current method for detecting energized objects is a two-step process. First, the area is "scanned" by a quite large, truck-carried detector; refer to Figure 2. The truck-carried detector covers large service areas within a small amount of time. But, it can only determine the existence of an energized object within a certain radius.

Figure 2. Mobile (truck-carried) scanner

To pinpoint the contact voltage (Step 2) a handheld meter is used. The handheld meter used historically was a Fluke meter with long leads and standard probes. Each object in the immediate area is suspect and has to be manually probed to locate the energized object. This process is time consuming. This is where the proposed new handheld detector should add significant time and cost savings to the detection process.

CHAPTER 3

EXISTING PATENT REVIEWS

Patent reviews are a critical step in almost any area of research. They ensure that the work being done is original, that the work is not a duplication of earlier work, and lastly, but most importantly, that one's own work avoids infringement upon another person's work. Several patents were reviewed to ensure that the methods and apparatus being developed were original in design and concept.

The following patents and brief descriptions from the review were found to be closely related to the claims in this thesis and the application for patents and therefore warranted close attention.

Vosteen, R.E. (1975) *U.S. Patent No. 3,873,919*. "AC Electric Fieldmeter." Washington, DC: U.S. Patent and Trademark Office

The primary claims of this patent are related to the ability to measure electric field intensity providing that there is no initial charge on the sensor and that the sensor is electrically isolated from the ground. In this patent's design two-plate sensors are used with a differential amplifier. The handheld device in this thesis operates with a single sensor and relies upon the ground. Also, it uses a single-ended amplifier configuration instead of a differential amplifier configuration. No real innovation exists in the approach described in this patent. It is well documented that the design represents prior art.

Knanishu, S.L. (1976) *U.S. Patent No. 3,993,951*. “Alternating Current Meter Circuit.” Washington, DC: U.S. Patent and Trademark Office

The key element of interest in this patent is the use of field effect transistors (FET) to provide high impedance in the order of 1015 kΩ. While the patent describes an alternating-current meter, the input is not defined. Different sensor types may be used to generate a current representative of the electric field. While this patent speaks of temperature errors and instability and prior art, the patent provides a means for stabilization of the circuit.

In the initial design concept it was proposed to use a high-input impedance amplifier stage to be able to collect charge. Research showed that this approach was not an effective means of detecting an electric field when in motion because of static buildup. Hence, it was determined that a stable amplifier such as those with high-input impedance of 1015 kΩ would be used. However, the amplifier configuration would be in the noninverting mode where impedance matching was performed at 60 Hz for the sensing element. The use of such an amplifier provides stability and very low input leakage that otherwise would introduce errors in the readings and does not conflict with the patent.

Tuszski, A.A. (1987) *U.S. Patent No. 4,646,002*. “Circuit for High Impedance Broad Band Probe.” Washington, DC: U.S. Patent and Trademark Office

The subject of interest in this patent is the art of high-impedance probe with low capacitance. The present design of the sensor head is a single element having quite low capacitance. This low-capacitance probe in the patent is necessary to prevent circuit loading. The signal is already weak and the additional capacitance of the probe further reduces the signal strength. The claims in this patent are similar to the claims for

the beta unit: high-impedance buffer circuit and capacitive circuit loading. But, the unit in this patent has instability problems. The concepts in this patent are related to direct-contact measurements of small circuits operating at high frequencies. On the other hand, the technology behind the beta unit is based on a large circuit area but uses an extremely small amount of stray capacitance to complete the circuit between the sensing element and the energized object.

Draaijer, M.H.J. (2000) U.S. Patent No. 6,051,967. “Electric Field Measurement System.” Washington, DC: U.S. Patent and Trademark Office

This patent is similar to U.S. Patent No. 3,873,919 and has similar claims regarding two sensor elements and high-input impedance differential amplifier. However, the main innovation is the use of fiber optics to transmit the detect magnitude providing isolation for high-voltage situations and to reduce errors form stray capacitance. The handheld detector in this thesis operates on the principle of a single sensor element and relies upon the ground. Also, the technology uses a single-ended amplifier configuration instead of a differential amplifier configuration. No real innovation exists in this approach as it is well documented to be prior art.

CHAPTER 4

TECHNOLOGICAL BASIS OF DETECTION BY EMISSION

After investigating the process of detecting energized objects in New York City as a Project Engineer/Scientist working for EPRI, I proposed a handheld emissions detector to replace the handheld Fluke voltmeter then being used to check all metal objects. At this early stage in research, my proposal was for a device that only "detected" (i.e., used the signal strength of the energized object's emission to locate it). Later, the concept would be expanded to make the device an "analyzer" capable of not only locating the energized object but determining the electrical condition that caused it to become energized.

The basis of the research effort for developing a handheld detector was predicted on the following assumptions:

- Energized objects are locatable by using a handheld detector that looks at object emissions.
- The condition causing the energized object could be identified by analyzing the harmonic signature of the object emissions.
- The use of the new handheld detector will be faster than the current method that uses a standard, handheld Fluke meter where every object in the vicinity has to be checked.

After the inadvertently energized object is located, it is necessary to determine the type of condition that is producing it. The condition type might be one of the following: (1) direct wiring contact, (2) energized earth contact, (3) induction coupling, (4) arcing, or (5) false positive–no energized object. More complete descriptions of the various causative conditions are shown next.

- Direct wiring contact: Energized object is a result of direct contact with an energized conductor.
- Energized earth contact: Energized object is a result of neutral return current from the overhead or secondary electrical distribution line serving the customer.
- Induction coupling: Energized object is a result of induction coupling—usually with overhead power lines.
- Arcing: Energized object is the result of a low-impedance fault that has not reached the level of catastrophic failure.
- False positive: No energized object. Emission comes from a switch mode power supply of a neon sign.

To identify the condition causing the energized object, the emission signal must be captured and analyzed. My original hypothesis was that each of the five conditions creating energized objects had a standard emission signature (i.e., harmonic pattern); refer to Table 1.

Table 1
Causative Conditions (i.e., conditions that can create an energized object) and Their Corresponding Harmonic Signature

Causative Condition	Harmonic Signature
Direct Wiring Contact	60-Hz sine wave with less than 5% THD
Energized Earth Contact	60-Hz sine wave with greater than 5% THD
Induction Coupling	Non-sinusoidal wave with third harmonic dominant
Arcing	60-Hz sine wave with noise detectable by 3rd derivative
False Positive	Sine wave with second harmonic > third harmonic

Appendix A provides further details concerning the identification of causative conditions for energized objects.

CHAPTER 5

PROPOSED HANDHELD DETECTOR

The proposed early-version of the handheld detector would still be used in conjunction with the truck-carried detector. And, its primary purpose is the same as the Fluke voltmeter—to “pinpoint” the location of energized objects. A Fluke meter would still be required to confirm the voltage of any detected, energized object.

The proposed emissions detector had a practical requirement of detecting an energized object to within 3 meters. This distance is chosen for two reasons, (1) a typical distance encountered on sidewalk is 3 meters and (2) a reasonable detection distance for an energized object exhibiting an electric field is 3 meters. Refer to Appendix B for further discussion on electric field decay. The mathematical principles behind detecting low-frequency electric fields, the associated wavelength of 60 Hz, and the effects of measurements in the near field are discussed in Appendix C.

The handheld detector has the advantage that it would speed up the pinpointing process while also adding the flexibility to search as close as possible to 100% of the immediate vicinity.

Early Versions of the Handheld Detector

Figure 3 shows the three earliest versions of the new handheld detector: (1) laboratory development (i.e., proof of concept), (2) alpha test detector–generation 1, and (3) alpha test detector–generation 2.

Figure 3. Chronological development of the new handheld detector

The term “alpha” is used to designate units *primarily* used in laboratory testing. All three of these early models were detectors only (i.e., they only had field-strength circuitry and LED indication).

Beta Version of the Handheld Detector

Like the early alpha units, the beta unit shown was a detector only; refer to Figure 4. The term “beta” is used to designate units *primarily* used in field testing. Like the alpha unit, it had no analysis circuitry to determine the cause of the energized object.

Figure 4. Beta version of handheld emissions detector

Sixteen beta detectors were laboratory constructed for use by the utilities in field testing.

CHAPTER 6

ADVANCEMENT OF DETECTOR TECHNOLOGY

A gamma unit (i.e., a large-quantity production model) was developed for this thesis. The gamma unit was the first unit to be both a detector and an analyzer. As stated previously, early versions (alpha and beta) were detectors only.

Requirements for the New Gamma Unit

After initial field trials with the alpha designs, the utility sponsors identified several requirements for the gamma unit.

- The detector should have lower power consumption with the capability of lasting 12 hours in between charges.
- It should operate with a single rechargeable 9-volt, lithium-ion battery—instead of the two chargers required for the alpha units.
- The charging should be simplified to a single connection.
- The case should be rugged, water-resistant, light weight, and made of nonconductive material.
- The indicator lights must be readable in the dark and during the day.

Using these requirements, the gamma unit was developed; refer to Figure 5.

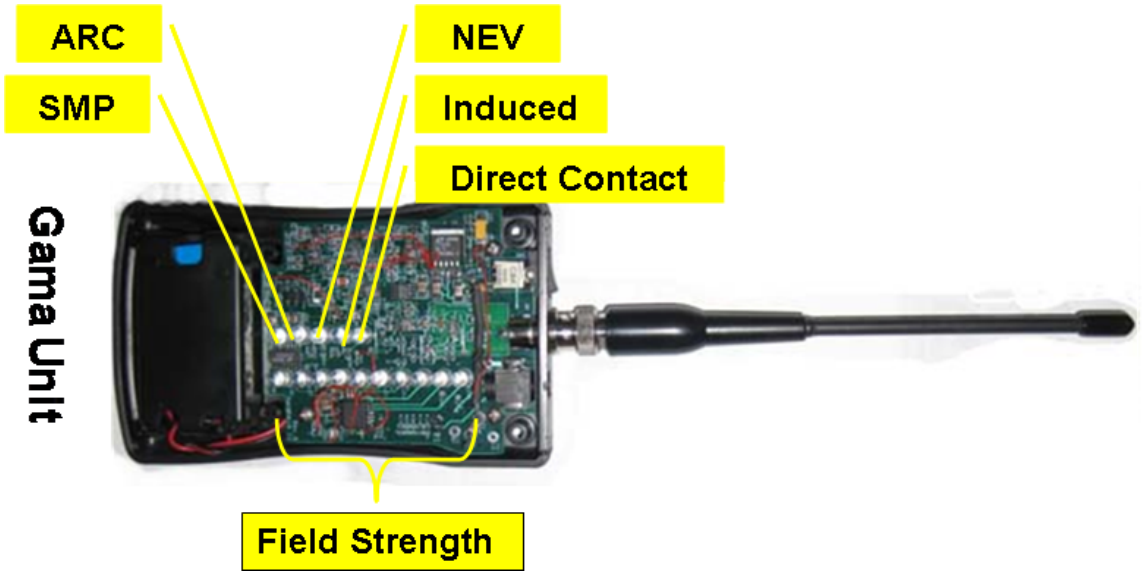

Figure 5. Circuit development for the gamma version of the new handheld detector

The remainder of this section provides descriptions of all the design activities and all the component selections involved in the development of the gamma unit: LED Indicators, Plastic Case Selection, Preliminary Circuit Design, Final Circuit Design, Sensor Head Selection, Circuit Design for Signal Amplifier, Circuit Design for Distortion Analysis and Fundamental Cancellation, Hardware Selection for the Analysis Circuitry, Gamma Unit Limitations, and Gamma Unit Production.

LED Indicators

On the gamma unit, two sets of LEDs are located on the front panel of the detector.

The first set of LEDs indicates the field strength. In earlier version of the handheld detector (i.e., alpha and beta), the LEDs displayed signal strength *linearly*. For increased sensitivity, a new LED display driver was designed for the gamma units. This new driver indicates signal strength *exponentially* (i.e., sensitivity decreases as the

signal strength increases which occurs when the detector is brought closer to the energized object).

The second set of LEDs is also located on the front panel. This grouping of five LEDs indicate the presence of either: (1) direct wiring contact, (2) energized earth contact, (3) induction coupling, (4) arcing, or (5) false positive.

Plastic Case Selection

To accommodate all the utility requirements, the gamma design was developed around the generic, off-the-shelf handheld package manufactured by Polycase® International; refer to Figure 6.

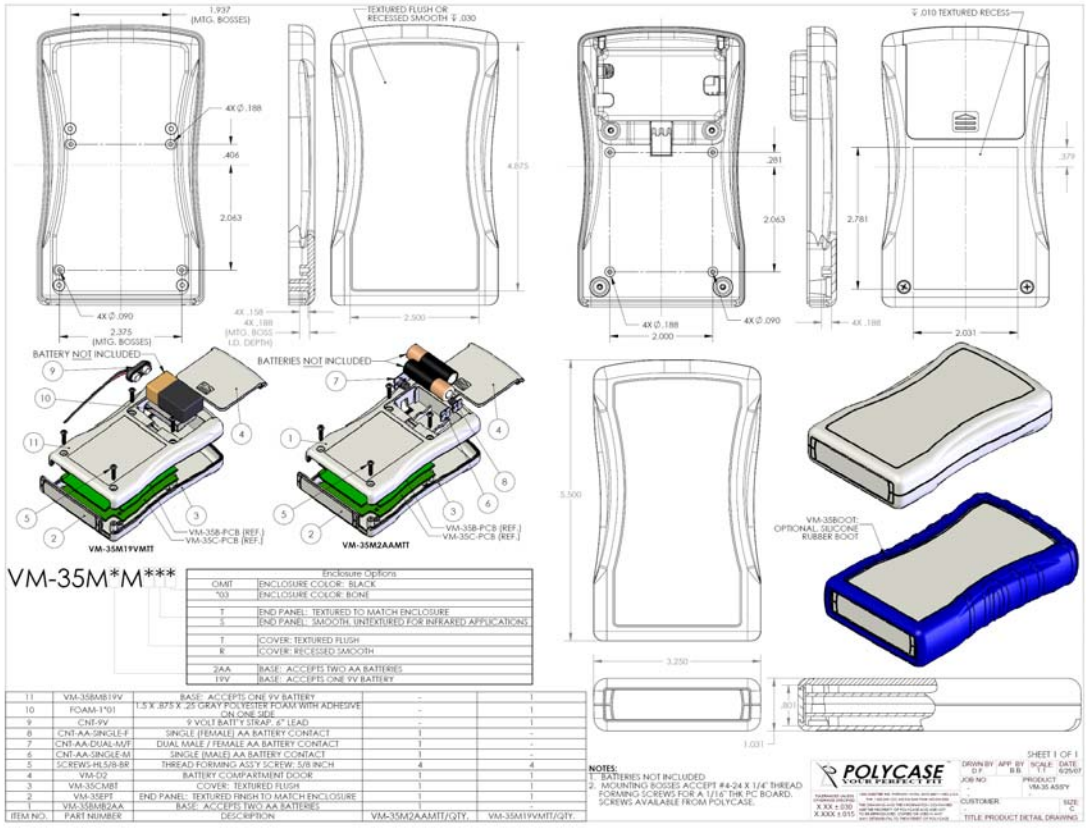

Figure 6. Polycase® specifications for generic, off-the-shelf electronics housing

Preliminary Circuit Design

The circuits for the gamma unit went through several design changes. While it was difficult to maintain a clean prototype on a breadboard a final circuit was finally constructed; refer to Figure 7. Then, a manufacturing layout and design was completed; refer to Figure *5*.

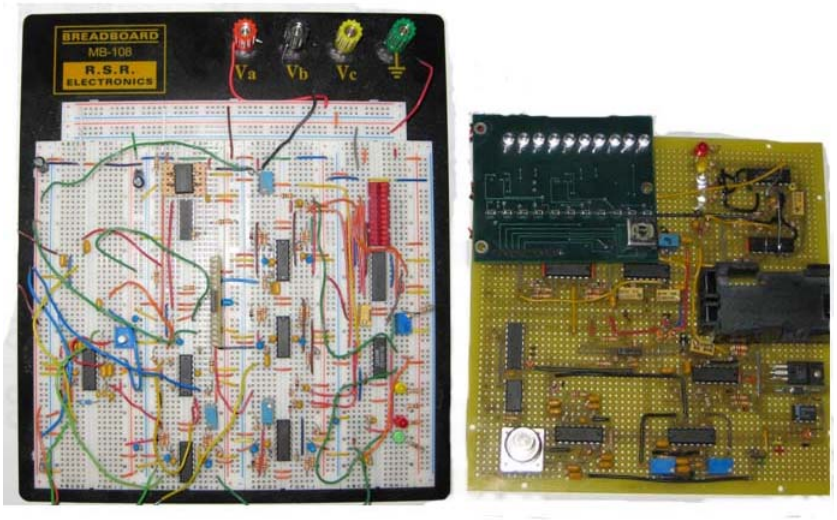

Breadboard **Protoboard**

Figure 7. Preliminary breadboard and protoboard for the gamma unit

Final Circuit Design

Figure 8 shows the basic analysis circuitry for the gamma unit from input (i.e., emission signal) to output (i.e., LED indication of causative condition for the energized object).

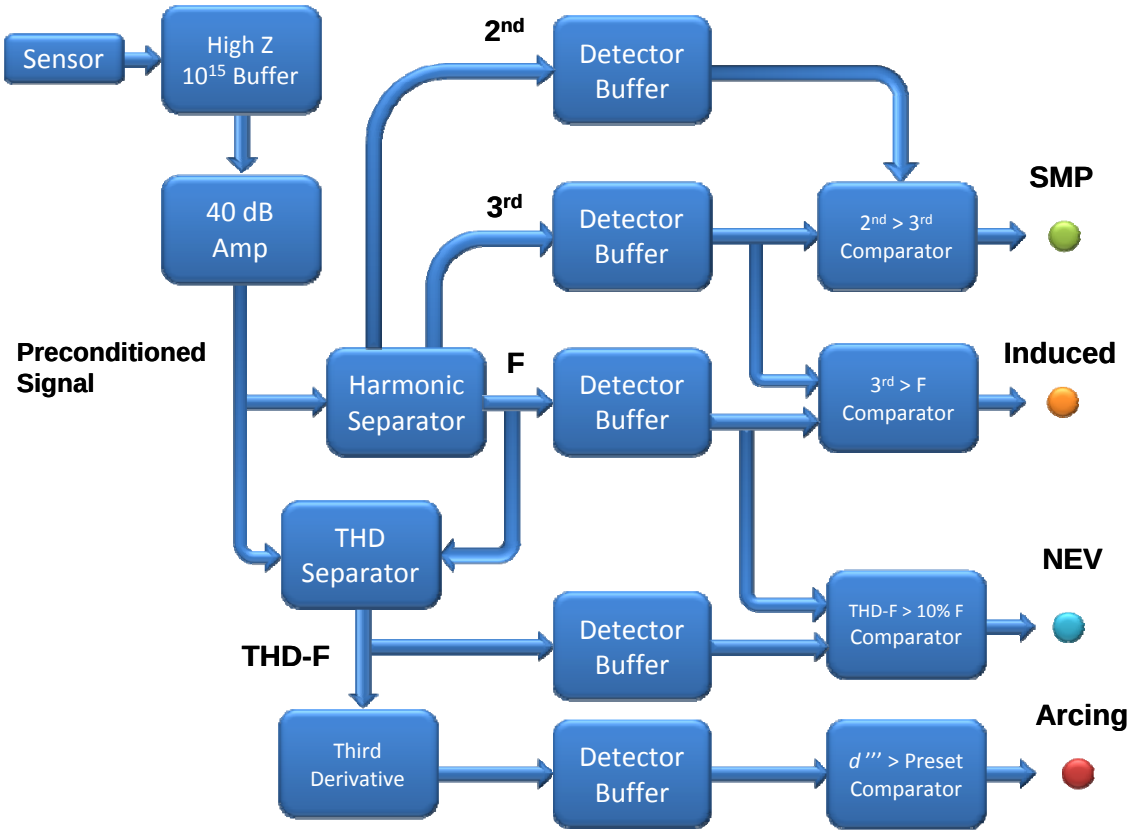

Figure 8. Circuit block diagram for gamma unit

Sensor Head Selection

The sensor head chosen for this project is a 800-MHz, monopole antenna. Appendix E covers the evaluation process for determining the best sensor for the application.

Circuit Design for Signal Amplifier

After the basic sensor head type was determined, an evaluation was performed to determine the best amplifier circuit (such as [1] single-ended, noninverted input, [2] single-ended inverted input or [3] differential input). To achieve impedance matching with the sensor head, the single-ended, inverted-input amplifier circuit was selected.

Initially, the signal is amplified by 40 dB (i.e., gain = 100) through four stages of amplification to maintain the necessary frequency response for arc detection and then fed directly into the THD separator and the fundamental canceller.

Circuit Design for Distortion Analysis and Fundamental Cancellation

The mixed signal total harmonic distortion analyzer (MSTHDA) provides highly filtered outputs of the fundamental frequency (60 Hz), the second harmonic (120 Hz), and the third harmonic (180 Hz). The filtered, 60-Hz fundamental is combined with the preconditioned signal to cancel out the 60-Hz component—leaving only the total harmonic and noise output. The fundamental canceller has two additional circuits that corrects for phase shift and level output to ensure complete cancellation of the fundamental frequency (60 Hz).

In the first step of signal analysis, the THD signal is compared against the 10% sample of the fundamental (60 Hz). When the THD root mean square (RMS) value is greater than 10% of the fundamental, the circuit activates the **energized earth** LED (shown as “NEV” in Figure 8).

The THD signal is passed through a third-derivative circuit. If the output exceeds a predetermined threshold, then the **arcing** LED (shown as “ARC” in Figure 8) is activated.

Then, the fundamental harmonic (60 Hz) is compared against the third harmonic (180 Hz). If the third harmonic is dominant, the **induction coupling** LED (shown as “Induced” in Figure 8) is activated.

The third harmonic (180 Hz) is compared against the second harmonic (120 Hz). If the second harmonic is dominant, then the **false positive** LED (shown as “SMP” in Figure 8) is activated.

Finally, the fundamental harmonic (60 Hz) is passed to the LED display driver circuit providing field readings in volts per meter (V/m). Once the handheld detector is sufficiently close to an energized object (i.e., 5 V/m), the direct contact LED is activated. A voltage to frequency converter is under design to be used to produce a corresponding audio output that is proportional to the field strength reading above 5 V/m.

Hardware Selection for the Analysis Circuitry

Once the circuit design was proven, the designs were transferred to surface-mount technology. Where possible, a SOIC–to–SIP adapter (where the acronym SOIC means small-outline integrated circuit and SIP means single-in-line package) was used for prototyping. This combination provided complete integration of surface technology with the single power supply. Refer to Appendix E for detailed circuit description and schematics.

Gamma Unit Limitations

While the new handheld detector is effective in detecting contact voltage, several sources (i.e., either incandescent or halogen store front lights and neon signs) may cause false positives. Refer to Appendix F for details regarding switch mode power supply false positive identifications and arc detection.

Neon signs are a source of false positives. A traditional neon sign will operate with a high-voltage AC source and produce large electric fields containing a fundamental 60-Hz frequency and associated harmonics.

Fortunately, neon signs are becoming a less common source of false positives. New switch-mode power supplies are the reason that they are becoming less of a problem. These new power supplies have a switching frequency (measured in 10s of kHz) with a modulation frequency of 120 Hz. The modulation frequency is caused by the full-wave rectification of the 60-Hz fundamental frequency of the line voltage. The prototype handheld detectors in this research have a limited frequency response of 60 Hz in the primary detector circuit. Thus, fewer false positives are encountered where the newer switch-mode power supplies and lighting circuits are encountered

Incandescent or halogen store front lights are the cause of false positive. In this case the electric field is not sufficiently cancelled because of the wider conductor spacing.

Incandescent store front lights are becoming less of a problem as they are replaced with energy-saving compact fluorescent lights and other technologies that use switch mode power supplies.

Gamma Unit Production

The gamma units have only been constructed in the laboratory in limited quantity for field evaluation with expected production units to be introduced in July of 2011.

CHAPTER 7

PROOF OF CONCEPT

The following sections describe and illustrate several key milestones in laboratory testing and field testing of the handheld emissions detector during a period of 2 years. Initially, a laboratory development model, an alpha unit–generation 1, and finally, an alpha unit–generation 2 were built for laboratory testing and initial field testing. Results of the alpha units were used to design and build beta units. Fifty beta units have been manufactured and are in the process of being distributed to the utilities for field testing.

The most recent testing has focused on the use of the gamma unit (i.e., production model) described in this thesis.

Laboratory Development Model–Laboratory Trial

The first unit constructed was crude and heavily modified as might be expected; refer to Figure 9.

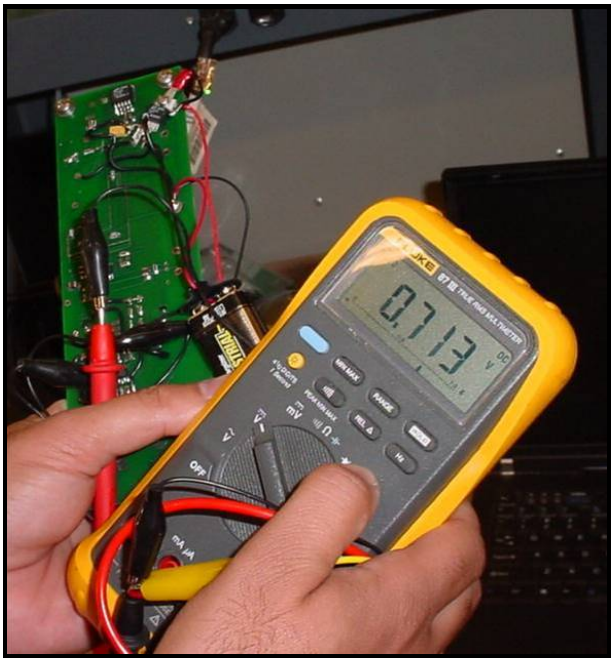

Figure 9. Performing output voltage check on the laboratory development model

With continued improvement, the laboratory development unit reached a level of refinement that an alpha test unit was built. Later, when a newer model was built, this first unit was called alpha test unit–generation 1. It was successfully evaluated with a 24-V_{AC} target in a copper screen room (used to block irrelevant external interference) in the laboratory; refer to Figure 10.

Figure 10. Laboratory development unit and 24- V_{AC} target

With successful testing in the laboratory, the laboratory development unit was taken to downtown Knoxville, Tennessee, and evaluated. There, similar false positives were detected that are found many times by the mobile, truck-carried system; refer to Figure 11. These early field trials led to the development of the alpha unit–generation 2.

Figure 11. False positive (caused by the switch-mode power supply for a neon sign) is detected by the early laboratory development detector

Alpha Unit–Field Trial

Normally alpha units are used only for laboratory testing. However, it was determined that the alpha units were sufficiently durable for field testing and that there was benefit to using the alpha units (generation 1 and 2) for initial field testing (i.e., before construction of the beta unit). While investigating various sites in New York City, the alpha unit was used in conjunction with the mobile, truck-carried system to pinpoint the location of an energized object. Figure 12 is an example of a site containing an energized storm drain and a traffic light energized at 23 V_{AC}.

Figure 12. Energized storm drain and traffic light

The series of photos in Figure 13 illustrates how the meter of the alpha unit–generation 1 begins to rise as an energized object is approached. In the upper left corner of the figure the energized storm drain and traffic light can be seen. In the right upper corner of the figure, the meter readout increases as the energized area becomes closer. Then, in the bottom left corner of the figure an even higher level of energization is shown. Finally, in the lower right corner of the figure, as the street corner is rounded,

the meter pegs to full scale at the traffic light. These energized objects were caused by a crushed service conduit with the line contacting the conduit underground.

Figure 13. Demonstration of increasing signal strength as an energized object is approached by an alpha unit–generation 1

At another location direct contact with the soil and pavement is verified with a Fluke meter; refer to Figure 14. The cause, in this case, is a previous patch made the prior year that has failed. What is important about this finding is that arcing was recorded on the voltage waveform similar to arcing recorded during a laboratory test with buried conductors.

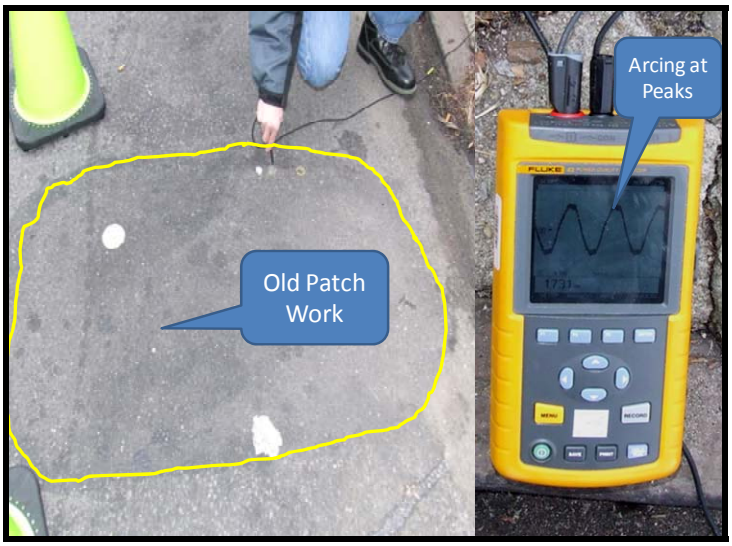

Figure 14. Energized area with arcing verified with Fluke meter

Beta Unit–Laboratory Trial

To improve upon the existing design, it is necessary to know the approximate field strength level being detected. With this information an accurate assessment of the performance levels and expected detection range can be made. The beta unit was calibrated using an E-field generator constructed of a parallel plate capacitor; refer to Figure 15.

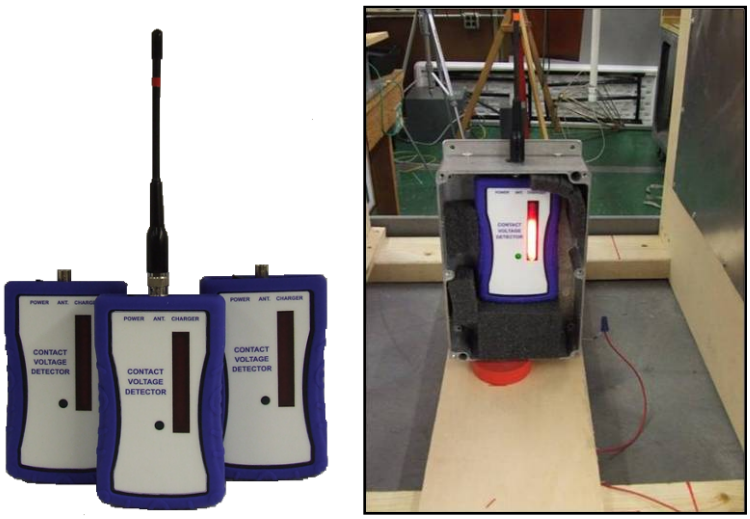

Figure 15. Beta unit and e-field laboratory verification

Beta Unit–Field Trial

The beta unit was field tested during various investigations such as (1) research on induction coupling between an overhead power line and a gas line, (2) research on energized object created by energized earth, and (3) research on mobile contact voltage detector.

As seen in Figure 16, an electric field is being emitted by the gas line under investigation. The gas line was identified and traced along the route of an overhead distribution line. Magnetic field mapping determined the highest points of induction coupling. Insulating pipe joints was recommended to reduce the voltage potential along the gas line.

Figure 16. Detection of induction coupling between an overhead power line and gas line

While performing a mobile scan using the research vehicle, the handheld detector clearly indicated an energized object more than 3 meters away. The cause of the problem was a bolt driven into the foundation of a traffic light that had broken the

insulation of the wiring. The immediate area was energized to a potential of 114.6 V_{AC}; refer to Figure 17.

Figure 17. Energized traffic light base cause by direct contact with electric wiring

During another scan an energized fence was detected at 27 V_{AC} as result of a bad overhead neutral. The handheld unit was able to detect the energized fence from within 3 meters of the fence. The causative condition was identified as energized earth; refer to Figure 18.

Figure 18. Energized fence caused by energized earth detected by a beta detector

CHAPTER 8

FUTURE STUDIES

A future study is a must to further the advancement of technology. In this application the next-generation handheld detectors will be center around PEDs, (portable electronic devices) such as the iPhone®, Android®, and other such devices that have highly integrated, digital signal processing (DSP) functions with powerful DSP microprocessors; refer to Figure 19.

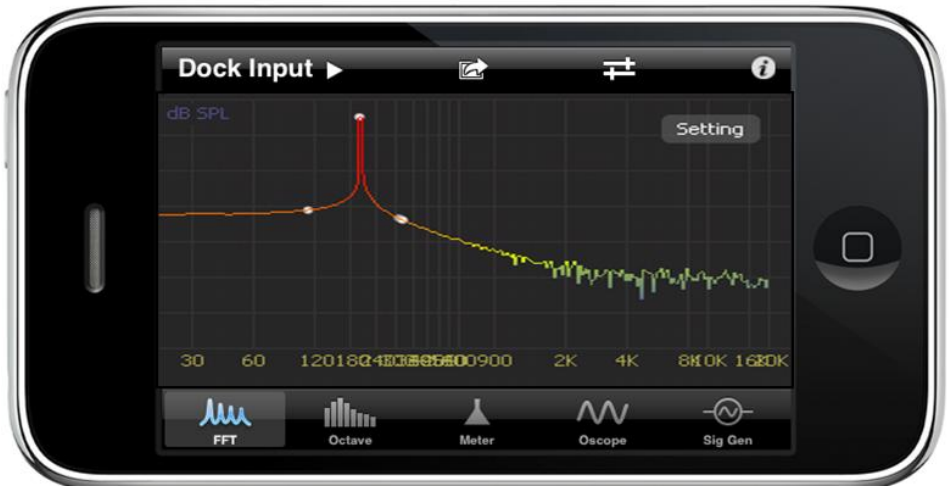

Figure 19. iPhone® displaying a Fast Fourier Transform

The data acquisition resolution of these devices is off the scale as compared to just 5 years ago. Currently they are able to provide 16- and 24-bit, digital two channels of audio up to 20-kHz and, in some cases, higher. They are also able to perform real-time Fast Fourier Transform (FFT) analysis in a reasonable processing time. These devices are equipped with manometers, accelerometers, and global positioning systems (GPS).

These features logging possible trouble spots and transmitting them back to the central control dispatch for further investigation.

With the appropriate front-end sensor, amplifier, and buffer, PEDs are the logical device for generation-X applications. With the computing power of PEDs, advance processing algorithms could be used to discriminate phase and detect electrified objects in the presence of overhead distribution lines. In the past the presence of overhead distribution lines would mask the characteristics of an electrified object. Techniques such as frequency-folding analysis could eliminate false positives caused by advance switch-mode power supplies.

CHAPTER 9

CONCLUSIONS

Through a program of laboratory testing, collected field data, raw waveforms, and actual field testing, the alpha and beta units have proven to be able to detect energized objects with the full range of emission signatures: (1) direct wiring contact, (2) energized earth, (3) induction coupling, and (4) arcing. The standard emission signatures (i.e., standard harmonic patterns) from the causative conditions have been identified. And, analog analysis circuits have been designed and incorporated in the gamma generation of the handheld unit—extending the capability of the unit and making it an analyzer.

Currently 50 production units are being manufactured and will be delivered to five utilities for further field evaluations in early spring of 2011. Manufacture of the new gamma version of the handheld detector is possible because key analog circuits and algorithms described in this thesis were patented and made available for low-cost licensing. The new gamma version of the detector that has been the focus of my research project and thesis offers improved speed of detection, simplicity, and low-cost of manufacture.

REFERENCES

Electric Power Research Institute (EPRI), (2003). “Distribution reliability indices tracking within the United States,” TR-1008459, San Jose, Calif.

Hanebuth, S. “Consolidated Edison stray voltage program,” 2010 PQA Conference, White Plains, NY.

IEEE 644, *IEEE Standard procedures for measurement of power frequency electric and magnetic fields from AC power lines*.

Jodie Lane Foundation, Manhattan Stray Voltage Map, http://strayvoltagenyc.org/manhattan-map, Retrieved Sept. 4, 2010.

Phipps K. Cooke, T., Dorr, D. & Keebler, P. (2010). “Frequency phenomenon and agorithms for arc detection,” IEEE EMC Symposium, July 2010.

Phipps, K., & Keebler, P. (2008). “Shielding with a twist,” IEEE EMC Symposium.

Schelkunoff S.A. (1943). *Electromagnetic Waves*. Princeton, NJ: Van Nostrand.

Sewell, C. (2006). “Con Ed finds 1,214 stray voltage sites in one year,” New York Times http://www.nytimes.com/2006/03/04/nyregion/04voltage.html?_r=1 Retrieved 18 Feb 2010.

Viemeister, P. E. (1972). *The nature of lightning and how to protect yourself from it-the lightning book*, Cambridge, MA. and London, England: The MIT Press.

APPENDICES

Appendix A

CONTACT VOLTAGE IDENTIFICATION

The fault (i.e., a high-impedance electrical short) can create electrical potentials between various objects that may or may not be embedded in the earth. These electrical potentials vary with environmental conditions and increase during periods of rain and snow melt. These faults are not observed or seen in an underground system. Thus, they are less likely to be detected until a person or an animal makes accidental contact.

After an energized object is detected, the utility scan team must then measure the voltage potential between the electrified object and a remote ground with a volt meter burdened with a 500-ohm resistor, (standard human impedance with a cut). If the detected electric field is created by electrostatic induction (i.e., by capacitive coupling), the use of the 500-ohm resistor will bleed off the voltage. If the potential of the energized object exceeds 1 V_{RMS} under burden and there is the possibility of human or animal contact, the situation must be repaired immediately.

The intent is not identifying the correct maintenance action, but to identify the causative condition that is being detected. The correct maintenance action is determined by the utility company based on the findings at the local site. To determine the maintenance action that must be taken by the utility company, the cause of the energized object must first be determined as (1) direct wiring contact, (2) energized earth, or (3) induction coupling.

When the Cause is Direct Wiring Contact

In the case of direct wiring contact, the high potential line on the distribution side has sustained an insulation breakdown that may be attributed to conditions such as area road construction and incidental deterioration of wiring insulation. Under these conditions, objects that are metallic—and even nonmetallic (such as pavement and concrete)—may become energized at any voltage level that is delivered by the distribution secondary system (i.e., 208 V_{AC} or 120 V_{AC}). Because the voltage is a result of contact with one or more wiring conductors, the primary frequency of the source voltage will always be the fundamental frequency of the power line (i.e., 60 Hz for North America).

To confirm that the emission from the energized object exhibits a fundamental frequency of 60 Hz in all North American cases, the human body model used by the International Electrotechnical Commission in standard IEC 60601-1 was constructed to be used in this research effort. It represents a standard burden when measuring the contact voltage to a remote ground; refer to Figure A-1.

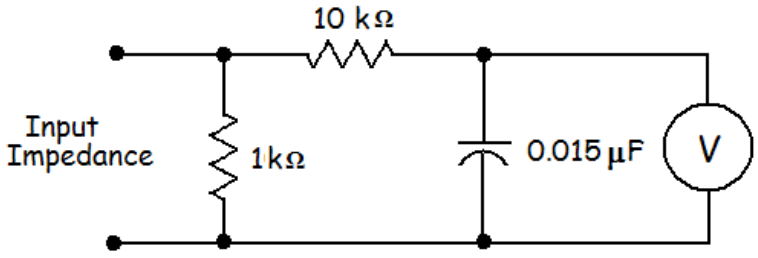

Figure A-1. Human body model of IEC 60601-1

The human body model was simulated with Multisim® software. Then, a test circuit with the required electrical components (i.e., a 10-kΩ resistor, a 1-kΩ resistor, and a 0.015-μF capacitor) was constructed in accordance with the human body model. The results from Multisim® were compared to the results of simulation with the physical test circuit with 1 Vrms stimulation. Figure A-2 shows little deviation in the required frequency response, while Figure A-3 shows positive results with the modeled current.

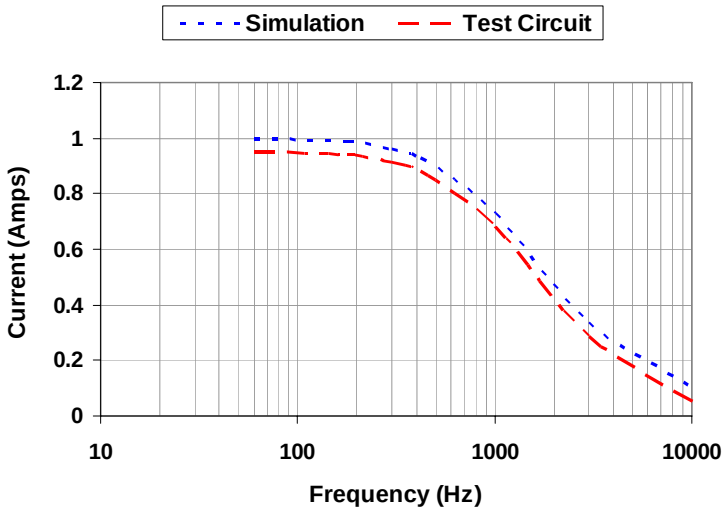

Figure A-2. Frequency response of the Multisim® model and the test circuit

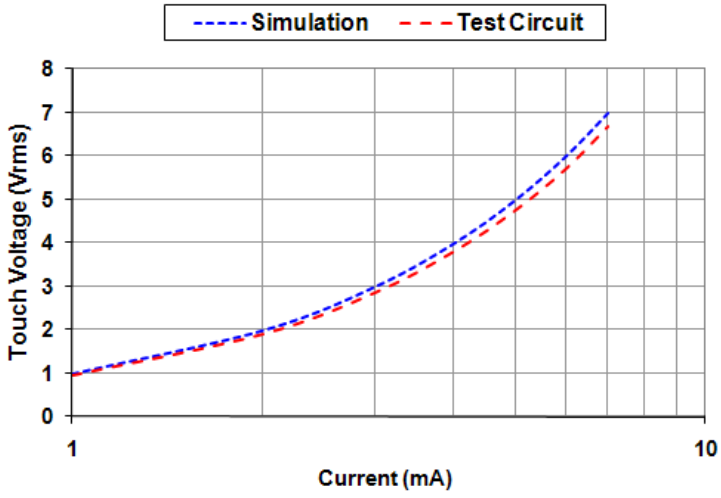

Figure A-3. Leakage current for the human body model

Four different soil mixtures were prepared to simulate typical and extreme soil conditions that may be found in New York City—the primary research area for this project. The four mixtures were:

Soil Mixture 1 – 50% clay, 25% sand, and 25% salt

Soil Mixture 2 – 75% sand and 25% salt

Soil Mixture 3 – 50% sand and 50% salt

Soil Mixture 4 – 100% sand

A low-voltage source was constructed using a variac and a low-voltage isolation transformer (i.e., 24- V_{AC}). The secondary of the transformer was connected to an electrode placed in the soil mixture on one side of the soil sample. One lead of a Fluke voltmeter with the ability to read true rms voltages was connected to another electrode placed in the soil sample; refer to Figure A-4

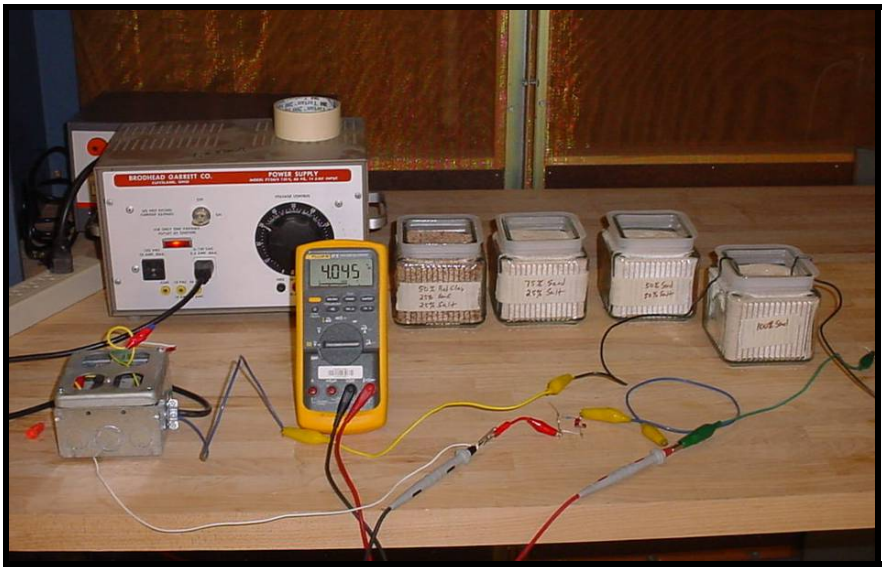

Figure A-4. Test Setup—Showing Variac, Fluke voltmeter, transformer, and samples of four soil mixtures

The next series of measurements included soaking the soil samples over time to simulate runoff water from snow melts and rain. For all instances the frequency of the voltage was 60 Hz. The voltage potentials differed between the human body model and the direct reading of the voltmeter for dry and wet samples indicating the need for a reasonable burden resistor, (1 kΩ @ 15 Watts) when verifying the contact voltage.

When the Source is Energized Earth

A unique characteristic of signals in many physical systems is harmonics. Power line harmonics are sinusoidal voltages or currents whose frequencies are integer multiples of the power-line fundament frequency of 60 Hz. The fundamental component is the first harmonic in a Fourier series of a periodic waveform; in this case 60 Hz.

Energized earth voltages are found on typical wye-grounded distribution systems. In this type of grounding system the neutral is grounded throughout the secondary system and is used as the primary return path back to the source. A portion of the return current will flow through the earth as the earth acts as a parallel conductor. Voltage potentials may be measured at any point along the current path with respect to a remote ground reference. The voltage measured with respect to this reference is referred to as neutral earth voltage.

In determination of neutral earth voltage, the total harmonic distortion (THD) of the voltage is used as the key indicator to determine if the measured voltage is a result of energized earth contact. According to EPRI distribution power quality (DPQ) studies, the typical THD of the power system voltage on the secondary side of a distribution system has a statistical mean of approximately 3% THD, (EPRI, 2003).

The THD is the ratio of the root-mean-square (RMS) of the first harmonic to the sum of root-mean-square value of all harmonics beyond the first (i.e., the sum of the second harmonic and all harmonics beyond). The mathematical expression for computing the THD is shown in Equation A-1.

$$THD = \frac{\sqrt{V2^2 + V3^2 + V4^2 + \cdots + Vn^2}}{V1} \quad \textbf{(A-1)}$$

Harmonics of the power frequency can be used to determine the condition causing the energized object. If the total harmonic distortion (THD) is less than 10%, than 90 % of the time the source of the electrification is direct wiring contact. If the THD is greater than 10%, then the source the electrification is energized earth.

Knowing the percentage of THD gives the utility worker a clue that the neutral earth voltage (NEV) may be related to the secondary side of the utility. The problem may reside at the customer premises when NEV total harmonic distortion is less than 30% but greater than 10%. As an example the voltage potential is being measured at a water line located close to a distribution line; refer to Figure A-5.

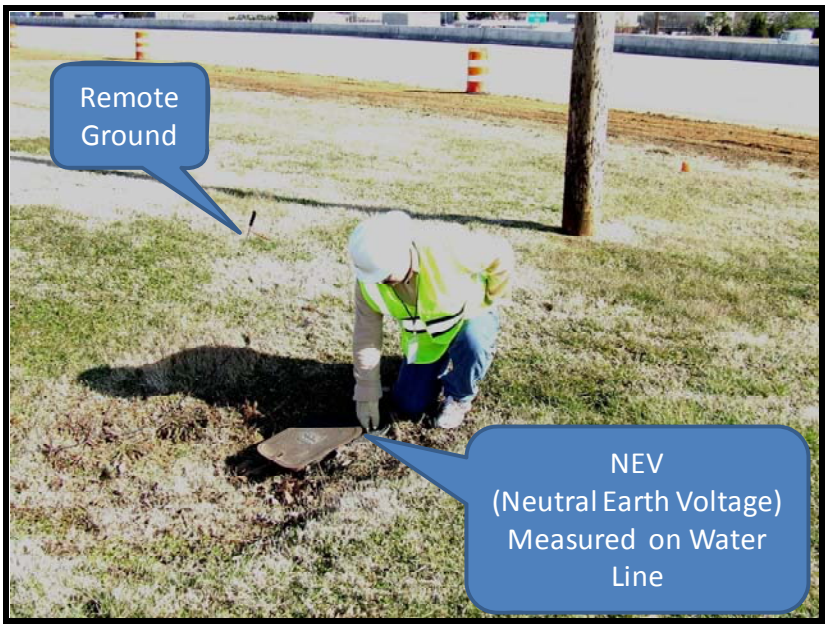

Figure A-5. NEV measurement on a water line

Figure A-6 shows that the voltage measurement is approximately 2 V_{RMS}, and repair action would be required if the THD level was lower than 10%. However, it is obvious that the waveform is not 60 Hz sinusoidal and is made mostly of 180 Hz, resulting in a THD value of 176% (Using the North American standards of computing THD, values greater than 100% can exist as the computation is based on the fundamental component magnitude and not the total value). Harmonic distortion levels of this magnitude are related to NEV and the problem is usually associated with the distribution neutral. As stated before the 3rd harmonic was found to be dominant—indicating an induced coupling condition or distribution return current as a result of the overhead distribution line and no repair action is required.

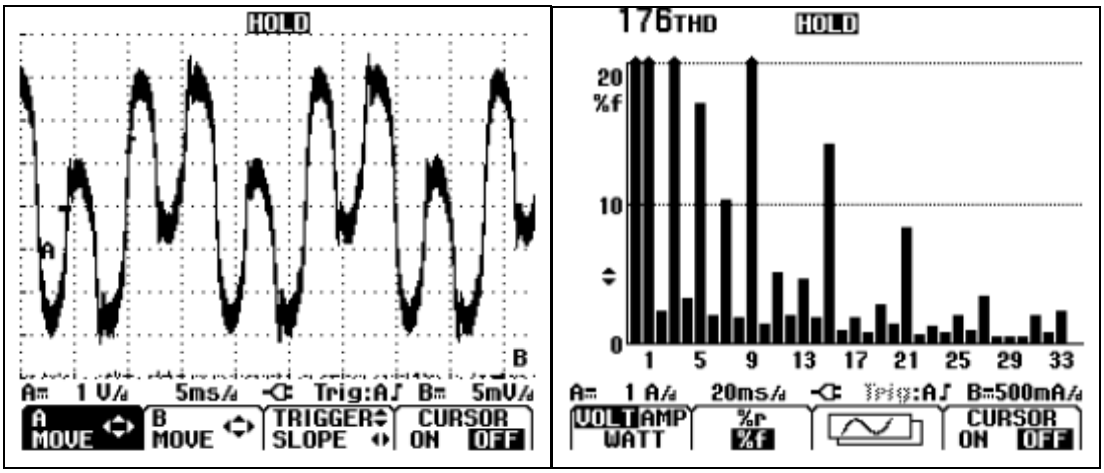

Figure A-6. Example of contact voltage caused by neutral return current (i.e., THD >10%). Note that the Fourier analysis shows a THD of 176%

In 2009 it was recommended that the New York utility companies start collecting data on the percent THD recorded for known contact voltages and causative conditions to substantiate the characteristics for direct wiring contact and energized earth. By the end of the third quarter of 2010, more than 3,000 recordings had been made. Figure A-7 shows two main trends. One is that voltages greater than 4.5 V_{RMS} are more likely to be attributable to direct contact. Second is the trend that THD values of greater than 5% are related to energized earth, (Neutral Problem).

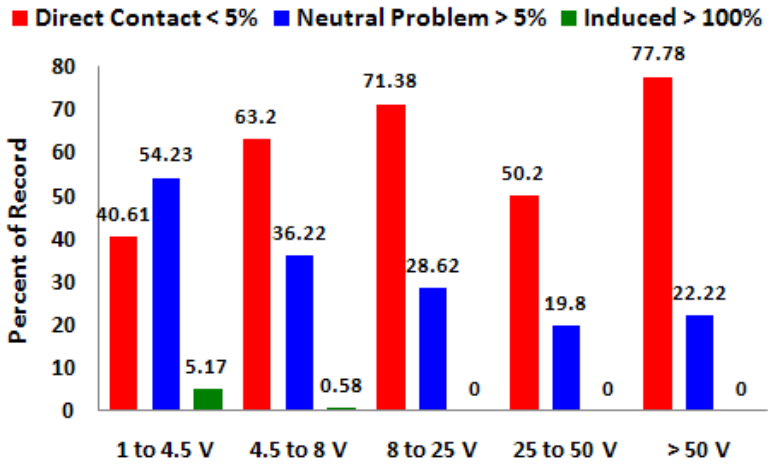

Figure A-7. Percent THD vs. problem

Another trend see is the fact that majority of the energized metal objects are attributable to direct wiring contact; refer to Figure A-8.

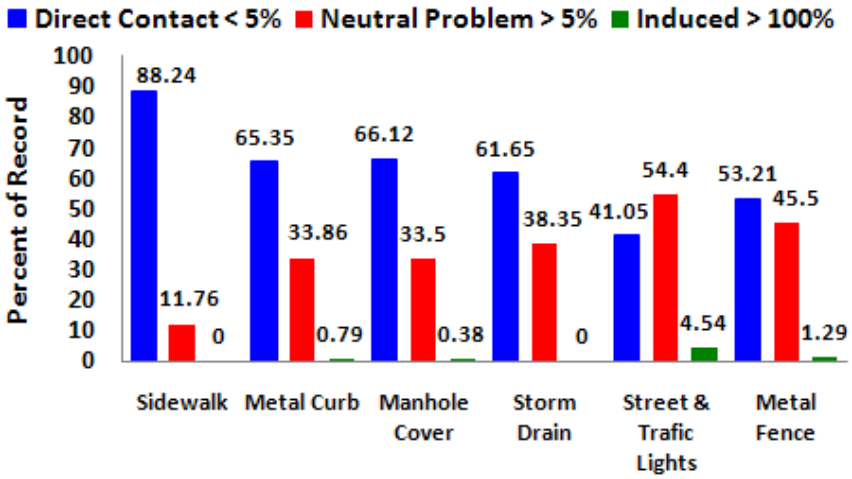

Figure A-8. Percent THD vs. object

Induction Coupling

Relative to contact voltage, electric transmission and distribution lines can induce voltages onto metal pipelines making them electrically conductive across long lengths.

The primary factors creating induced voltage include unbalance phase currents, high neutral currents, or currents flowing on shield wires. For streetlight poles, traffic cross arms, fences, and other metal objects, inadvertent energization can be a concern if the object is in close proximity to the power distribution lines.

Figure A-9 shows a gas meter that has approximately 20 V_{AC} of induced voltage between the customer side and the utility side of the meter. This is a result of the gas line being run in the same right away as a three-phase distribution power line.

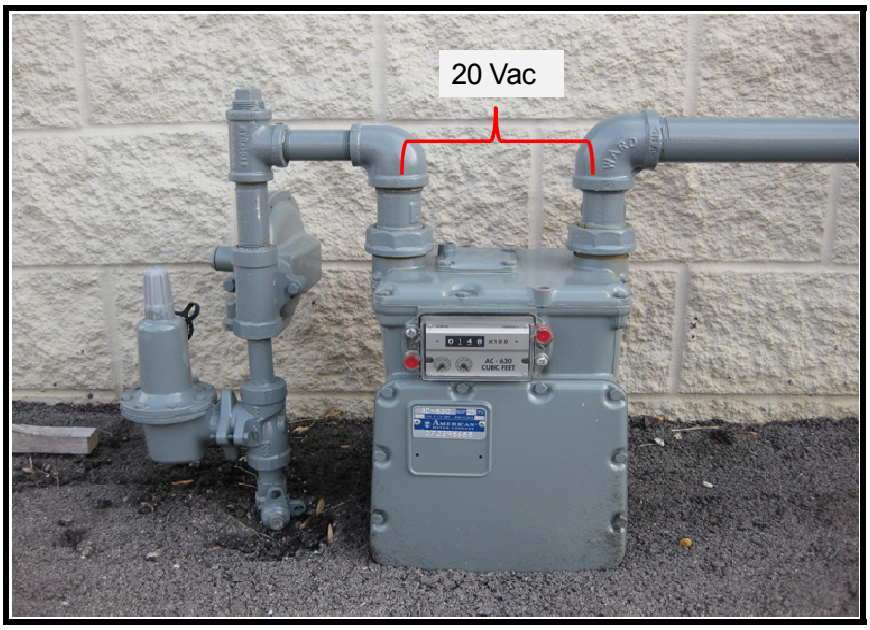

Figure A-9. Gas meter with induction coupling

A three-phase power line voltage contains multiple harmonics of the fundamental frequency of 60-Hz power. To characterize the voltage profile from magnetic induction, a long loop was erected beneath a distribution line and the resulting voltage was recorded; refer to Figure A-10.

Figure A-10. Characterizing measurement of induced voltage with a loop

As shown by the largest frequency bin in the FFT in Figure A-11 the 180-Hz harmonic component is the dominant harmonic for a typical induced voltage.

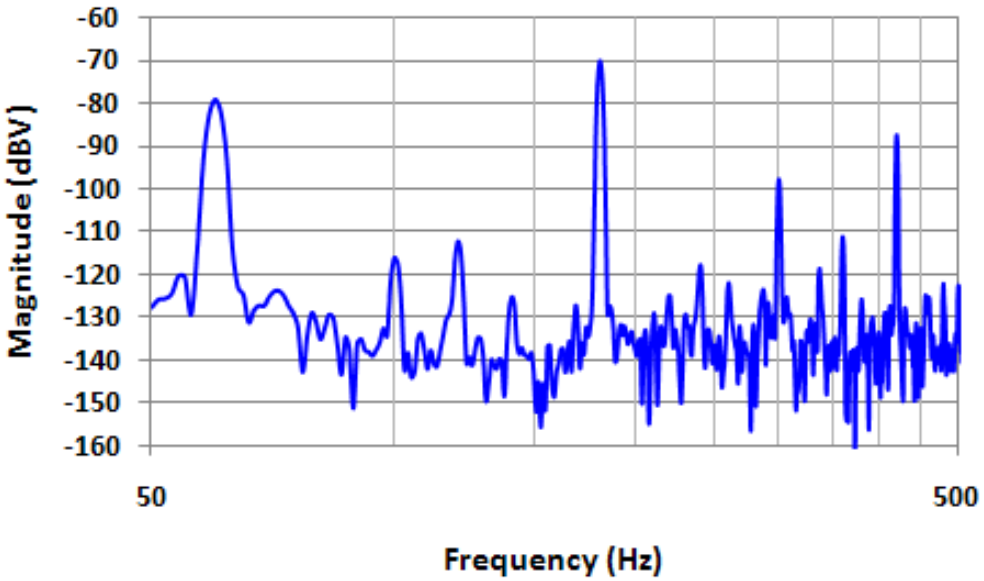

Figure A-11. Frequency spectrum of an Induced Voltage. The dominant frequency (i.e., largest peak) is 180 Hz

The fundamental 60-Hz frequency is almost cancelled because of the phase relationship of the three-phase power system. The phase relationship in the time domain is 120° between the three phases. The fundamental frequency cancels because of the alignment of the three phases in space, (geometry of the lines) and time. The odd harmonics (i.e., first, third, fifth, and so on) are positive sequence and are additive in time instead of canceling—resulting in a dominant frequency of 180 Hz.

Appendix B

ELECTRIC FIELD CHARACTERISTIC BEHAVIOR

During this research effort it became apparent upfront that the sponsor and interested parties needed to understand the concepts of near field and far field behavior of the electromagnetic field in these two conditions, in particular the near field.

Appendix D discusses the determination of far field and near field based on wavelength. This appendix discusses the mathematics behind field behavior in simple terms of a simple dipole antenna as the target or field targets are perceived to act as an electrically small dipole antenna with the image pole being the earth.

Next, laboratory data are provided in support of the characteristic behavior of the field strength falling at a rate of $1/r^3$ and not 1/r terms that is understood by the majority of electrical engineers lending to confusing in the understanding of the expected field strength verses distance from an energized object.

Electric Field Characteristics of a Dipole Antenna

During World War II early Russian studies of ground wave propagation introduced the world to a new set of electromagnetic physicists. Escaping Russia during World War II, Russian mathematician S.A. Schelkunoff came to America and published an important text book, *Electromagnetic Waves* published by Van Nostrand in 1943. This textbook provides the fundamental background for the currently accepted principles of electromagnetic waves and modern antenna theory (Phipps 2008).

Schelkunoff defined the characteristics of a dipole antenna using Maxwell's equation, refer to Equation B-1 where:

E_θ = Electric field for time varying charge V/m

l = dipole element length in meters

β = electrical length per meter, $\frac{2\pi}{\lambda}$

ω = angular frequency, $2\pi f$

$\varepsilon_\circ$ = permittivity at point of interface to free space, $\frac{l}{36}\times 10^{-9}$ F/m

$$E_\theta = \frac{I l \beta^3}{4\pi\omega\varepsilon_\circ}\left[\frac{-j}{(\beta r)^3}+\frac{1}{(\beta r)^2}+\frac{j}{\beta r}\right]\sin\theta e^{-j\beta r}\ V/m \qquad \textbf{(B-1)}$$

However, it can be seen that the initial concept can now be simplified or reduced to basic algebraic terms by ignoring scale factors and constants, refer to Equation B-2.

$$y=\left[\frac{1}{r^3}+\frac{1}{r^2}+\frac{1}{r}\right] \qquad \textbf{(B-2)}$$

By plotting the basic 1/r terms (i.e., 1/r, $1/r^2$, ands $1/r^3$) in Equation B-2, it can be seen in Figure B-1 that the $1/r^3$ term is dominant in the near field and all of the other terms fall off as the distance approaches zero.

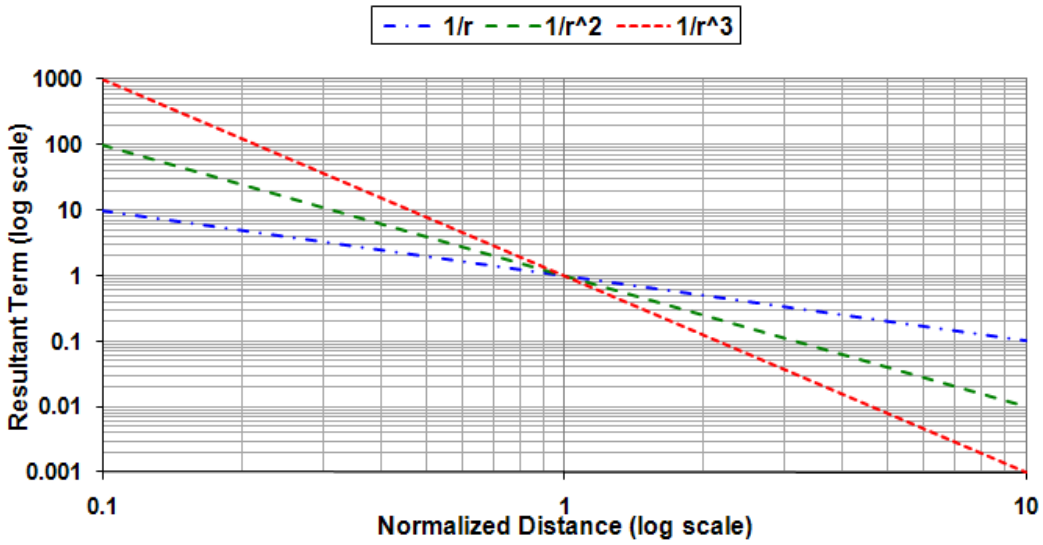

Figure B-1. Illustration of 1/r terms (i.e., 1/r, 1/r2, ands 1/r3)

Considering the measurement distance and the electrical wavelength of the time-varying field of 60 Hz, it is apparent that electric field decay rate behaves as a $1/r^3$ function. Knowing the proper decay rate of the electric field is an important factor in design of the final detector. The electric field at varying distances from the energized object may be estimated and accounted for in the required sensitivity of the handheld unit.

Electric Field Behavior of Laboratory Target: Open Area Test Site

Often, in emissions testing an open area test site (OATS) is required because of: (1) the existence of reflections inside a test chamber and/or (2) the equipment under test is too large to fit within the test chamber.

The immediate area outside of the electromagnetic compatibility (EMC) lab located in EPRI Building 2 in Knoxville is one such area that has been determined to be electrically quiet and suitable to perform open area testing.

To ensure that theoretical data are supported by actual data, it is desirable to map the electric field generated by an energized object. The target (i.e., the box on casters with pvc-encased antenna) is seen on the left in Figure B-2 at the OATS.

Figure B-2. Open area test site (OATS) and 3-meter target on the left

In Figure B-3, the electric field can be seen falling off as a function of distance and exhibits the typical omni-directional field pattern of a monopole antenna. If the target where to be scanned from bottom to top, the shape would be that of a doughnut.

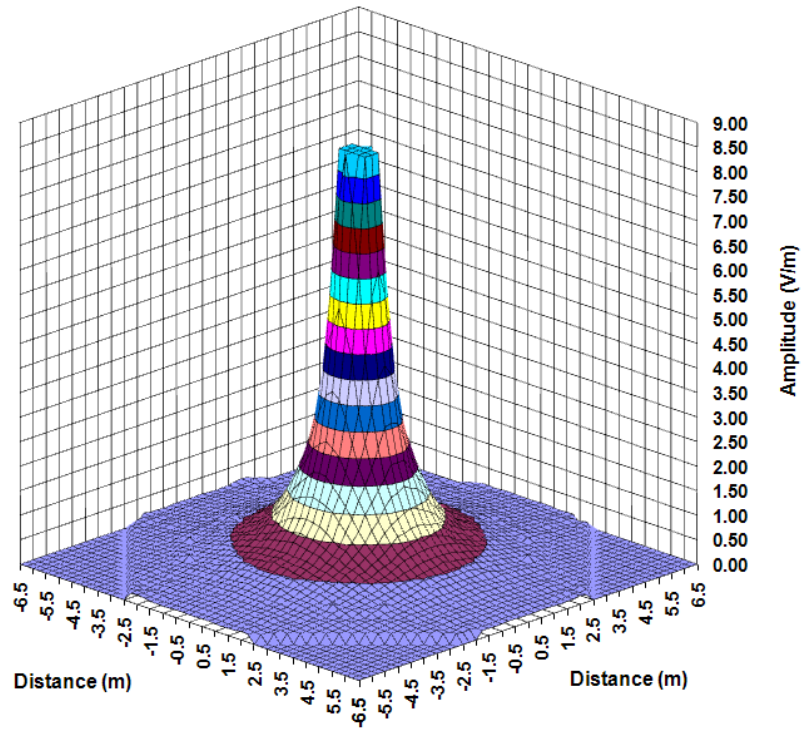

Figure B-3. Electric field plot of the 3-meter target energized at 12 V_{AC}

Figure B-4 illustrates the agreement of the $1/r^3$ function as discussed and supports the analytic theory used in this research project.

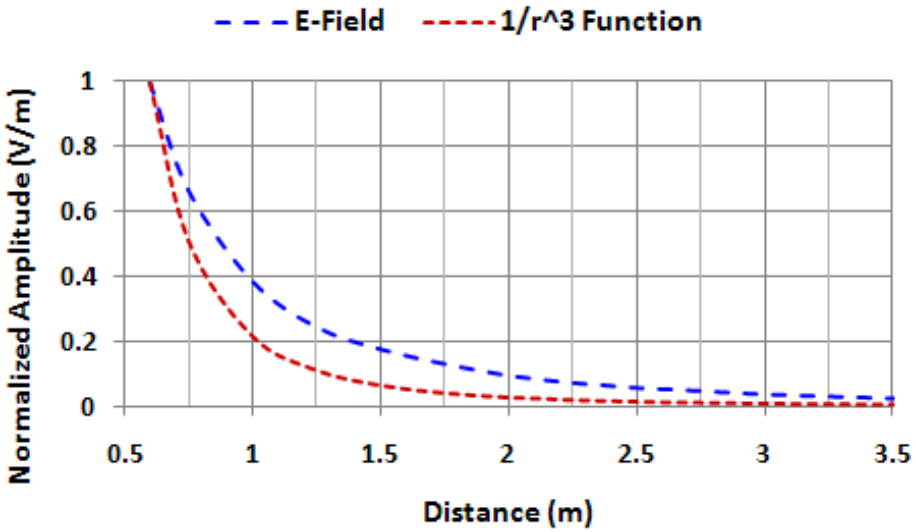

Figure B-4. Decay of the electric field is compared to $1/r^3$ function

Appendix C

MATHEMATICAL BASIS OF NEW HANDHELD DETECTOR

Common urban street objects energized by a distribution power line emit an electric field with characteristics that can be sensed and analyzed by the new handheld detector.

The nature of the electric field at different distances from an energized object was characterized; refer to Figure C-1.

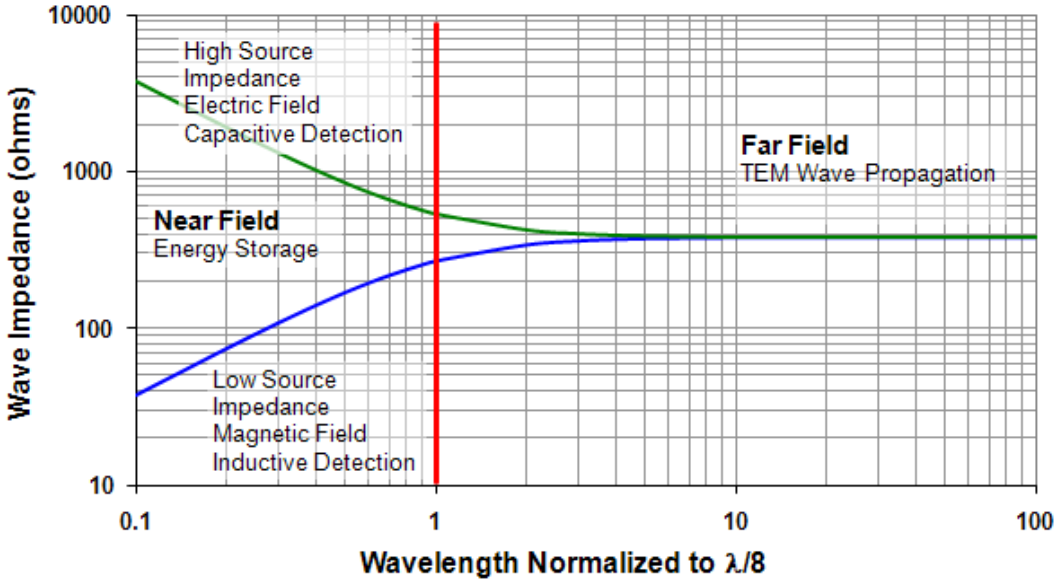

Figure C-1. Near field and far field regions as distinguished by the field delimiter (i.e., the normalized wavelength)

Note that the characteristic of the emitted electric field are completely different before and after the field delimiter. The field delimiter can be calculated as λ/8. The two primary regions seen in Figure C-1 are the near field and far field.

In this study energized objects are expected to be detected within 3 meters by the new handheld detector. It is necessary to determine if the handheld detector

operating within the 3-meter detection limit will be detecting near field conditions only or a combination of near field and far field conditions. To make this assessment, it is necessary to determine the field delineator and then compare it to the typical 3-meter detection distance. Step 1 is to determine the wavelength of standard 60-Hz power.

Wavelength Calculation for Standard 60-Hertz Power

The wavelength *(λ)* of any electromagnetic wave radiation can be calculated using Equation C-1 (i.e., the basic wavelength equation).

$$\lambda = \frac{c}{f} \qquad \textbf{(C-1)}$$

Where:

λ = wavelength (in m)

c = speed of light (a constant at 3×10^8 m/s)

f = frequency (in 1/second)

The wavelength for a standard 60-Hertz power line is calculated by substituting known values into Equation 3. The phase velocity (c) approximates the speed of light in free air space and is given as 3×10^8 m/s. The frequency (*f*) is 60 Hz (or the Hertz equivalent 60 cycles per second).

$$\lambda = \frac{3x10^8 m/s}{\frac{60}{s}} \quad \text{or, specifically} \quad \lambda = 5x10^6 m$$

The wavelength of the emission from a 60-Hz power line or energized object is shown to be 5×10^6 (i.e., 5000 kilometers).

Use of Wavelength to Determine Detection Method

Because the wavelength of 60-Hz power is 5000 kilometers, the field delineator ($\lambda/8$) between near-field and far-field conditions can be calculated as 625 kilometer.

As stated earlier, energized objects are expected to be detected within 3 meters of the energized object by the new handheld detector. This normal 3-meter detection distance is well within near-field condition as determined by the field delineator distance of 625 kilometers. Thus, the detector will be operating completely in near field conditions and not a combination of near field and far field conditions.

Principle Behind the Selected Detection Method.

The basic premise of detection is based on capacitance, which can be defined as the ratio of voltage to charge as defined in Equation C-2.

$$C = Q / V \quad \textbf{(C-2)}$$

Where:

C = capacitance in Coulombs/volt (or alternatively in Farads)

Q = charge in Coulombs

V = potential or volts

In the traditional sense, capacitance is only applied to objects that are relatively close together. In the urban situations encountered, the objects are reasonably distant and the capacitance is very small.

In the current thesis research the sensor technology is capacitive. The physics of detection is based on electrostatic induction. It is the electric field that occurs

between two charge-holding bodies to which the handheld unit responds. The sensing element (antenna) and the energized object act as the parallel plates of a capacitor with parasitic capacitance, capacitance as result of the proximity to other conducting objects or mediums completing the circuit.

Neglecting the parasitic and fringing effects, the capacitance (C) of a standard parallel-plate capacitor of area (A), plate spacing (d), and dielectric constant (K_o) can be determined by Equation C-3:

$$C = (K_O A) d \quad \textbf{(C-3)}$$

The charge (Q) can be determined from Equation C-4:

$$Q = CV \quad \textbf{(C-4)}$$

Then, the surface charge density (σ) can be determined from Equations C-5–C-8:

$$\sigma = Q/A = C/A \quad \textbf{(C-5)}$$

$$V = (K_O A/Ad) \quad \textbf{(C-6)}$$

$$V = (K_O V) d \quad \textbf{(C-7)}$$

$$V/d = \sigma/K_o \quad \textbf{(C-8)}$$

The electric field intensity ($\vec{E}$) is directional and perpendicular to the sensing element (antenna) and is defined by Equations C-9 and C-10.

$$\vec{E} = V/d \quad \textbf{(C-9)}$$

$$\vec{E} = \sigma/K_O \quad \textbf{(C-10)}$$

For a standard parallel-plate capacitor with area (A) and charge density (σ), the total induced charge (Q) is calculated in Equation C-11 and C-12:

$$Q = \sigma A \quad \textbf{(C-11)}$$

by substituting $\sigma = K_O E$

$$Q = K_O \vec{E} A \quad \textbf{(C-12)}$$

Because K_o and A are constants, the charge induced on the sensing element (antenna) is directly proportional to the electric field intensity of the energized object.

Detection in a Real-World, Multiple-Capacitance Environment

As just discovered, the charge induced on the sensing element is proportional to the electric field intensity. The question that now arises is how does the sensor detect the charge in an urban environment where there are multiple charges and parasitic capacitances as seen in Figure C-2.

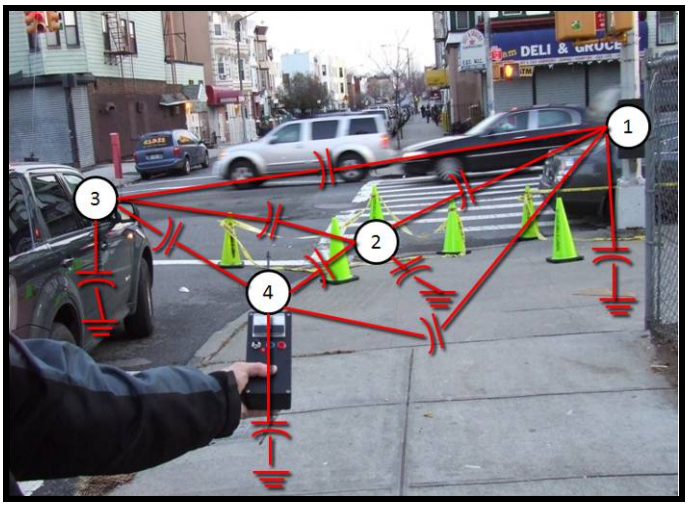

Figure C-2. Multiple capacitive objects in typical urban environment

The concept of the basic parallel-plate capacitor is extended to a region having multiple conducting bodies such as found in an urban environment. In Figure C-3, a number of conducting bodies of various geometries exist with the earth chosen as a zero reference (Plonsey, 1961).

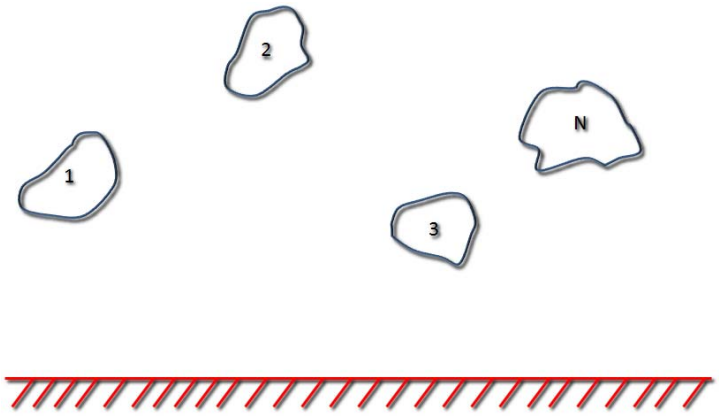

Figure C-3. Multiple charged bodies

The uniqueness theorem as applied to Laplace's equations for boundary conditions basically states that a charge on a body while the earth is held at a zero reference has a potential that is unique to that body and determines the potential everywhere in respect to that body (Plonsey, 1961).

Because of the linear dependence of the potential charges, the following Equations C-13–C-22 can be derived:

Where:

Φ is the absolute potential of charge

p is the coefficient of potential and depends on geometry

q is the total charge on the object

$$\Phi_1 = p_{11}q_1 + p_{12}q_2 + \ldots + p_{1N}q_N \quad \textbf{(C-13)}$$

$$\Phi_2 = p_{21}q_1 + p_{22}q_2 + \ldots + p_{2N}q_N \quad \textbf{(C-14)}$$

Therefore:

$$\Phi_N = p_{11}q_1 + p_{N2}q_2 + \ldots + p_{NN}q_N \quad \textbf{(D-15)}$$

The terms of p_{ij}'s in the above set of equations are constants and are referred to as the coefficients of potential and depend only on geometry of the object. From Equation C-15, we can see that the potential on each object is a function of the total charge on each and has a linear relationship.

The N term equations then can be solved to give the charges as a function of potentials and yield the following Equations C-16–C-18:

$$q_1 = c_{11}\Phi_1 + c_{12}\Phi_2 + \ldots + c_{1N}\Phi_N \quad \textbf{(C-16)}$$

$$q_2 = c_{21}\Phi_1 + c_{22}\Phi_2 + \ldots + c_{2N}\Phi_N \quad \textbf{(C-17)}$$

Therefore:

$$q_N = c_{N1}\Phi_1 + c_{N2}\Phi_2 + \ldots + c_{NN}\Phi_N \quad \textbf{(C-18)}$$

The terms of c_{ij}'s depend only on the terms of p_{ij}'s, and only depend on the geometry of the object as well. The terms of $c_{11}, c_{22}, \ldots c_{NN}$ are known as coefficients of capacitance, and the terms of c_{12}, c_{13},...etc. are coefficients of induction.

Because the coefficients of induction must satisfy the condition of reciprocity (i.e., $p_{ij} = p_{ji}$ and $c_{ij} = c_{ji}$), Equation C-18 can be rewritten with $C_{ij} = -c_{ij}$ while C_{ij} will be positive as $(i \neq j)$ then:

$$C_{ij} = c_{i1} + c_{i2} + c_{i3} + \ldots + c_{iN} \quad \textbf{(C-19)}$$

By adding and subtracting terms Equation C-19 becomes:

$$q_1 = C_{11}\Phi_1 + C_{12}(\Phi_1 - \Phi_2) + C_{13}(\Phi_1 - \Phi_3)\ldots + C_{1N}(\Phi_1 - \Phi_N) \quad \textbf{(C-20)}$$

$$q_2 = C_{21}(\Phi_2 - \Phi_1) + C_{22}\Phi_2 + C_{22}(\Phi_1 - \Phi_3)\ldots + C_{2N}(\Phi_2 - \Phi_N) \quad \textbf{(C-21)}$$

Therefore:

$$Q_N = C_{N1}(\Phi_N - \Phi_1)_{\,2} + C_{N2}(\Phi_N - \Phi_2) + C_{N3}(\Phi_N - \Phi_3)\ \ldots + C_{N2}\Phi_N \quad \textbf{(C-22)}$$

A portion of the total charge $C_{12}(\Phi_1 - \Phi_2)$ on object 1, (defined as the detector) depends on the difference of potential with object 2. Correspondingly, on object 2, and because $C_{12} = C_{21}$, an equal but opposite charge is bound. This corresponds to the view that objects 1 and 2 are connected by a capacitance C_{12}. Of the total charge on object 1, portions are bound on the remaining capacitors connecting to object 1 with every other object, and the remaining charge is found on capacitor C_{11} with the corresponding potential Φ_1 with respect to ground. This concept is illustrated in Figure C-4. Because of the complexity of this model, precision measurements are not as important as directivity.

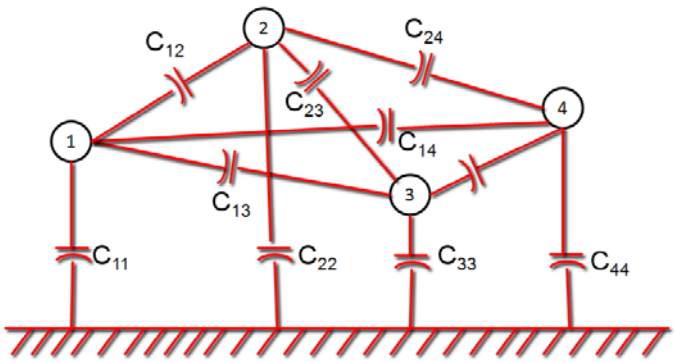

Figure C-4. Multiple capacitances to ground

Appendix D

DETERMINING FINAL SENSOR HEAD DESIGN

A variety of possible sensor heads are available for experimentation. However, it is desirable to keep the sensor head as simple as possible to minimize cost. Therefore, it is necessary to gain maximum sensitivity and directivity while maintaining a relative low physical profile.

A basic test setup was constructed with 24 V_{AC} applied to a 1.8-m section of 1.9-cm copper pipe contained within an insulating PVC pipe. The target was suspended in a brass-screened, electric field–isolation room to minimize interference from external 60-Hz electric fields; refer to Figure D-1.

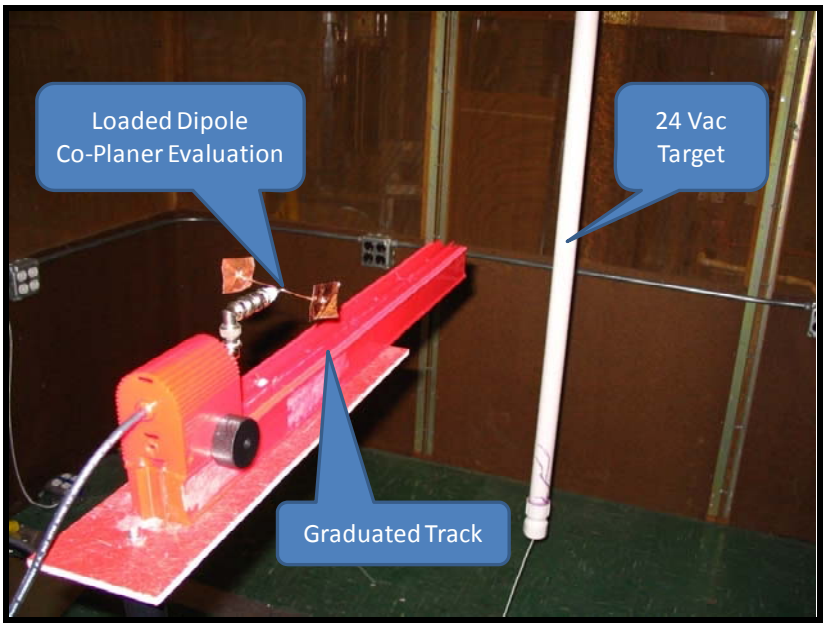

Figure D-1. Target test setup within a screen room

The voltage applied to the target (i.e., the1.8-m section of 1.9-cm. copper pipe insulated with a 3.8-cm PVC pipe) was supplied by a small filament transformer whose

source cable was screened using interlocking-armor cable fed back to the power source of the screen room.

The transformer was installed inside an aluminum enclosure to minimize the electric field generated by the transformer. The relative, electric field (not defined in terms of V/m) was measured by using a low-frequency network analyzer (a Stanford Research, Model SRS 780 in this case). Refer to Table 2, performance summary for various antenna and sensor performance.

Table 2
Performance Summary for Various Antenna and Sensor Plates

Size and Description	15 cm Standard Monopole	53 cm Whip	30 cm Monopole	15 cm PCB Monopole	4 cm Loaded Dipole	4.75 cm PCB Loaded Dipole	7.5 cm Full Load Dipole	7.5 cm Square Plate	5 cm Square Plate
Measured with 24 Vrms Target (dBV)	14.1	15.2	15.1	14.9	1.6	2.5	14.8	15	14.9
Compared to 15 cm Monopole (%)	100	108	107	106	11	65	18	106	106
Z @ 60 Hz (MΩ)	220	140	210	205	170	210	125	110	100

From Table 2, three sensor types were chosen for further evaluation. Experiments were performed on three basic designs that had performed similarly in the

test setup: (1) a capacitive-loaded dipole element, (2) a simple plate, and (3) a generic monopole antenna used for 800-MHz scanners, refer to Figure D-2.

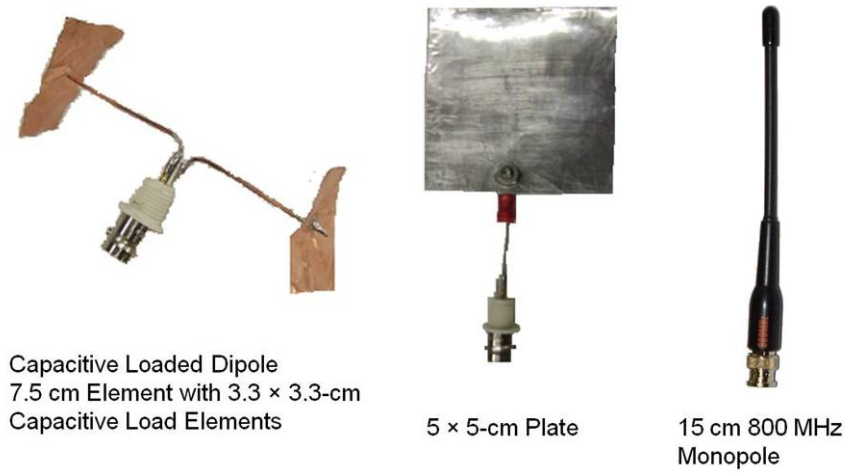

Figure D-2. Candidate sensor head types

As seen in Figure D-3, all three sensor types perform very similar in the basic test.

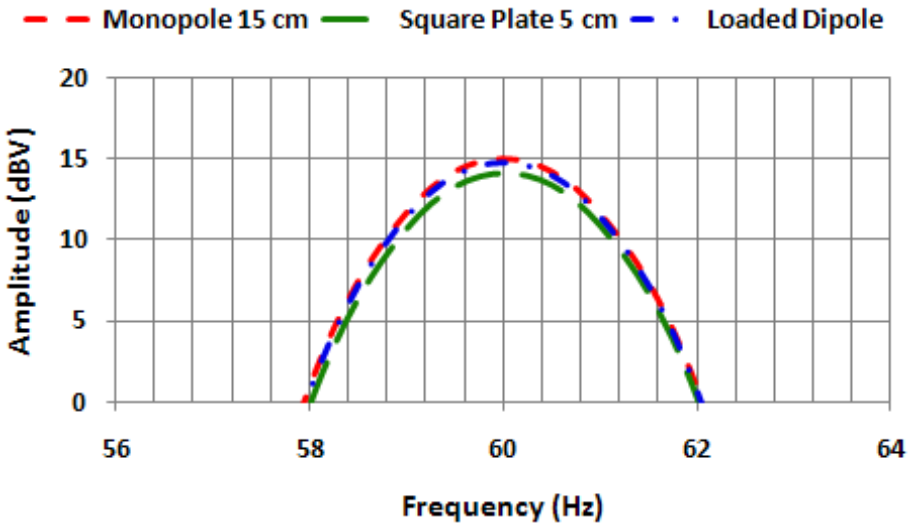

Figure D-3. Performance comparison of three sensor types to target with 24-Vrms stimulation

Using the test setup in Figure D-1, a directivity test was also performed by rotating the sensor from the center of target to the left and to the right. This test

revealed that the monopole antenna had more directivity than the 5 cm square plate; refer to Figure D-4.

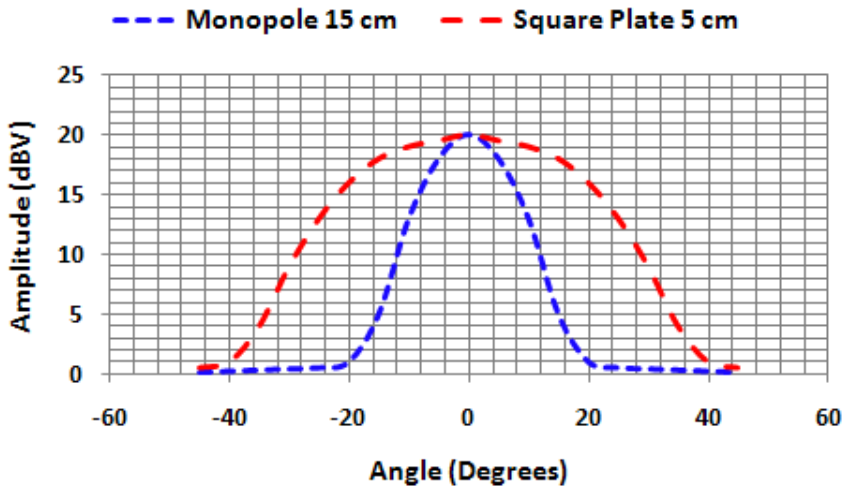

Figure D-4. Monopole directivity. Signal strength decreases as the monopole antenna is rotated to the left and right from the center of the target

Controlled Electric Field Generation: Parallel Plate Capacitor

When a metallic object or structure is energized, it acts as a single plate of a capacitor. For calibration and verification of the sensors it is necessary to establish a controlled baseline to measure performance and sensitivity of the sensors.

A parallel-plate capacitor was fabricated for calibration of the electric field sensor and also to gain an understanding of the behavior of the coupling mechanism to be encounter in the field.

Figure D-5 shows two 0.5×0.5 m capacitor plates separated by a distance of 0.5 m. Indents were built in the test setup to allow the spacing of the plates to be adjusted from 0.25 m to 0.75 m in five equal steps. Varying the plate separation allowed the study of (1) the effects of fringing fields on the sensor and (2) the relative accuracy of the sensor within a uniform and nonuniform field.

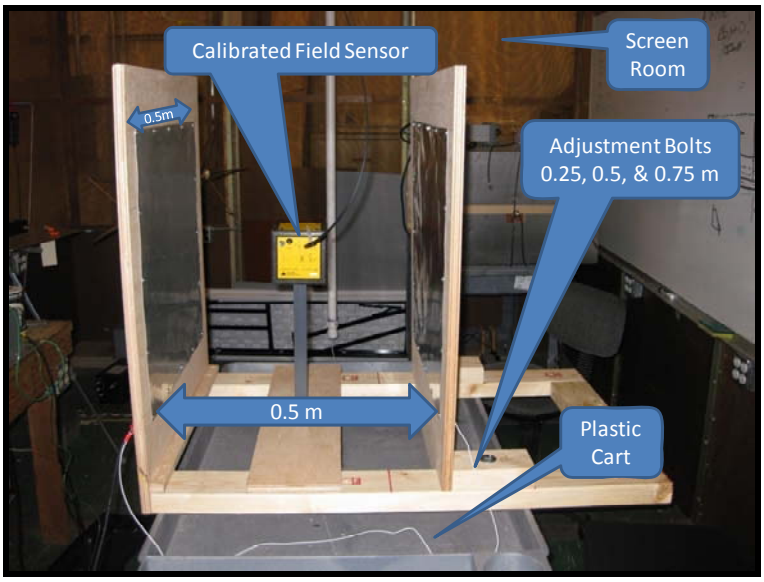

Figure D-5. Test setup with Hewlett Packard 33120A signal generator and a parallel-plate capacitor

The calculated field of a parallel-plate capacitor is given by Equation D-1.

$$V/m = \frac{V}{d} \qquad \textbf{(D-1)}$$

The calculated and measured electric field values are seen in Table 3.

Table 3
Calculated and Measured Electric Field Data for Parallel-Plate Capacitor

Plate Voltage d= 0.5m	Calculated (V/m)	Measured (V/m)
0.5	1	1.02
1	2	2.28
1.5	3	3.33
2	4	4.42
2.5	5	5.38
3	6	6.34
3.5	7	7.33
4	8	8.28
4.5	9	9.25
5	10	10.21
Correlation		0.999349

Next, see Figure D-6. This figure illustrates reasonable agreement between the calculated and measured value of the field strength.

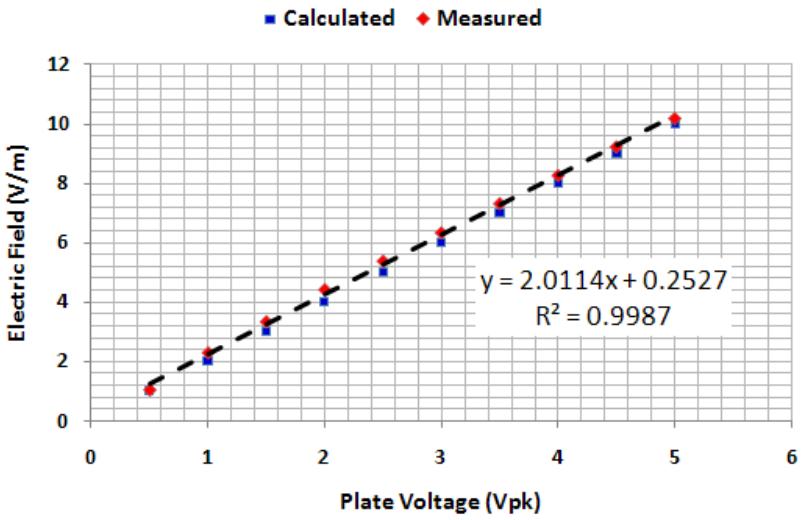

Figure D-6. Calculated and measured e-field of the parallel-plate capacitor

The electric field strength was measured using a calibrated NARDA, EFA-300 low-frequency electric field sensor. The measured values of the electric field strength are well within the 10% deviation allowable by IEEE Standard 644, entitled *IEEE Standard Procedures for Measurement of Power Frequency Electric and Magnetic Fields from AC Power Lines*.

Sensor Response Using a Parallel-Plate Capacitor

Once the parallel plate capacitor E-field generator was verified for accuracy using a laboratory-grade e-field sensor, the next step was to confirm the linearity of the amplifier output stage and to establish a baseline for the field strength reading from the beta handheld unit. Table 4 shows the amplifier output voltage level for e-field strengths between 0.5 and 10 V/m and the sine wave amplitude of the amplifier output signal in volts peak to peak (Vpp) and volts root mean square (V_{RMS}).

Table 4
Monopole Antenna Performance Under Parallel-Plate Test

V/m	Vpp	Vrms
0.5	0.12	0.039
1	0.216	0.071
1.5	0.332	0.112
2	0.438	0.146
2.5	0.582	0.180
3	0.642	0.218
3.5	0.754	0.256
4	0.886	0.291
4.5	0.960	0.327
5	1.08	0.366
5.5	1.18	0.403
6	1.28	0.437
6.5	1.4	0.477
7	1.5	0.509
7.5	1.65	0.555
8	1.75	0.592
8.5	1.84	0.625
9	1.95	0.661
9.5	2.06	0.701
10	2.18	0.737

As expected, the amplifier output is directly proportional to the field strength from 0.5 to 10 V/m with a correlation coefficient of 0.999 indicating an almost perfect linear output as seen in Figure D-7. The best-fit line equation is shown in the graph along with the calculated correlation coefficient (R^2).

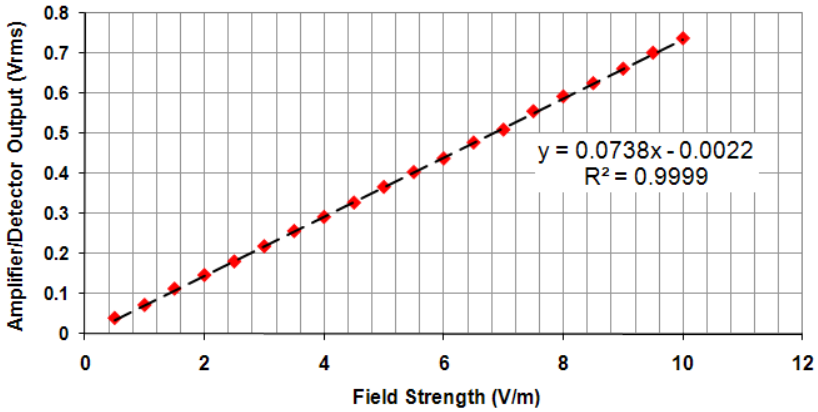

Figure D-7. Amplifier linearity graph

Defining The Monopole Antenna in Terms of Surface Area

The 15-cm monopole 800 MHz scanner antenna is available commercially from Radio-Shack and out-performs the other two sensor types evaluated based on directivity. It also outperforms the much larger electromagnetic compatibility (EMC) Mil-Std 104-cm. rod antenna used for electromagnetic compatibility (EMC) in MIL-STD-461F.

To further understand this phenomenal performance, it was desirable to make assessments based upon surface area and determine the surface area of an equivalent performing square plate.

Figure D-8 shows the dimensions of the 800-MHz monopole antenna. For calculation purposes the antenna was divided into three segments.

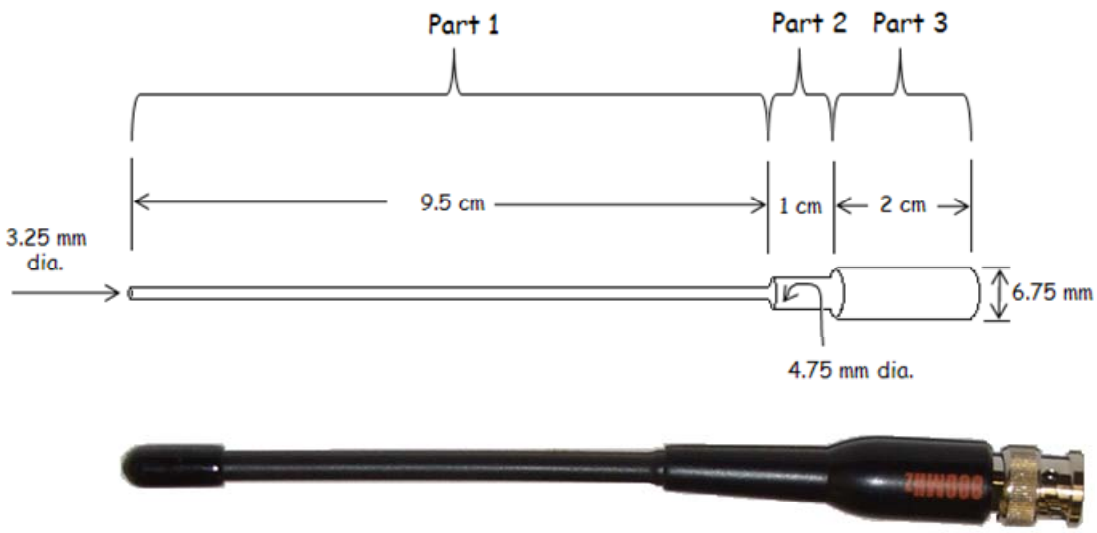

Figure D-8. Photo of 800-MHz monopole antenna along with its dimensions

The surface area of each segment was computed by using Equations D-2–D-3. The area of the three segments were summed and their total equals the total surface area of the antenna. Equation E-1 was used for calculating segments 1 and 3, and Equation D-3 was used to calculate segment 2.

$$Area = 2\pi r^2 + 2\pi rh \quad \textbf{(D-2)}$$

$$Area = \pi r^2 + 2\pi rh \quad \textbf{(D-3)}$$

where

r= radius

h= height

Thus

Segment 1 area = 1.658 + 96.990 = 98.649 cm^2

Segment 2 area = 3.544 + 149.22 = 184.66 cm^2

Segment 3 area = 7.156 + 424.11 = 495.67 cm^2

Total Surface Area = 166.7 cm^2

Surface Area Verification of Monopole Antenna

Evaluations were conducted by using a parallel-plate E-Field generator and several cut sections of an aluminum sheet; refer to Figure D-9.

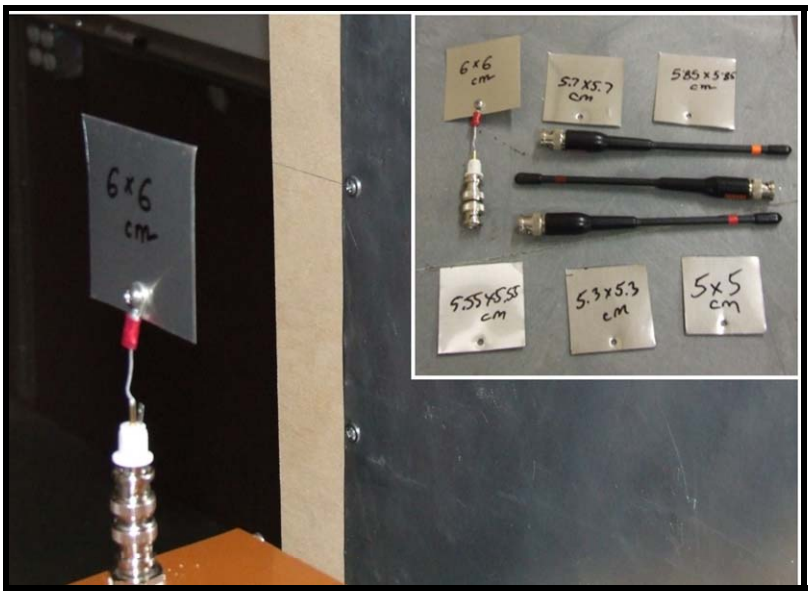

Figure D-9. Photo of 15-cm monopole antennas and plates of various sizes

By using an amplifier, signal generator, oscilloscope, and the parallel-plate capacitor, a reference value of signal amplitude was established at 60 Hz for the 15-cm monopole antenna. Next, a square plate made from an aluminum sheet cut to dimension of 6×6 cm was used in the test setup. Additional plates of various sizes were substituted until the output magnitude was relatively close to that of the 15-cm monopole antenna. The total surface area is approximately two times the surface area of one side.

Table 5
Plate Size vs. Measured Voltage

Sensor Type	Surface Area ($cm^{2)}$	Measured Voltage (Vrms)			
15-cm Monopole	166.7	0.500	1.000	2.000	3.000
5×5 cm plate	50.00	0.420	0.970	1.960	2.920
5.3×5.3 cm plate	56.18	0.512	1.040	2.120	3.060
5.5×5.5 cm plate	60.16	0.528	1.060	2.160	3.200
5.7×5.7cm plate	64.98	0.536	1.100	2.240	3.320
5.85×5.85 cm plate	68,44	0.544	1.120	2.260	3.360
6.0×6.0 cm plate	72	0.560	1.140	2.320	3.420

From Table 5, notice that the plate that matches the surface area of the monopole antenna would be closest the 5.3×5.3 cm plate with surface area of 56.18 cm^2.

The best-fit linear expression for each voltage level is derived from plotting the measured voltage vs. surface area for each test level; refer to Figure D-10.

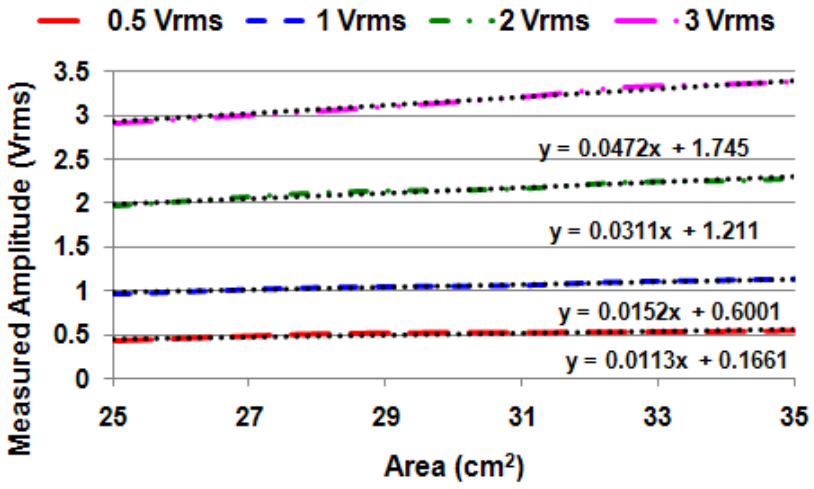

Figure D-10. Surface area vs. measured voltage

Next, the coefficients are averaged along with the expected resultant, and the resulting Equation D-4 is solved for the best-fit surface area:

3 = 0.0472x + 1.745

2 = 0.0311x + 1.211

1 = 0.0152x + 0.6001

0.5 = 0.0113x + 0.1661

1.625 = .0262x +0.93055 **(D-4)**

Solving for x yields: 52.64 cm^2 or a 5.13 cm square plate, including the two sides.

The calculated value of the surface area of the monopole antenna was 52.64 cm^2, while the measured and computed plate equivalent was approximately 25 cm^2. This difference in surface area and the explained performance of the monopole is attributed to the fact that when the plate is placed within the calibrated field both sides of the plate are exposed, resulting in a total surface area of 50 cm^2 instead of 25 cm^2. In practice a flat plate would only be exposed on one side contributing to the lower performance as compared to the monopole antenna.

Determining Electric Field Coupling Behavior

Because there is a significant difference in surface area of the monopole antenna and the computed and measured surface area of the plate equivalent, another method or experiment had to be derived to gain a full understanding of the sensor head coupling mechanism.

It is well established in the field of electrostatics that charges concentrate on the point of a sharp object. Benjamin Franklin once wrote, “There is something, however, in the experiments of points, sending off or drawing on the electrical fire, which has not been fully explained…I am of the opinion that houses, ships, and even towers and

churches may be effectually secured from the stroke of lightning by their means…there should be a rod of iron eight or ten feet in length, sharpen to a point like a needle, and gilt to prevent rusting, or divided into a number of points, which would be better…" (Viemeister, 1972).

Benjamin Franklin was able to reason this concept of electrostatics without the aid of modern equipment. Fortunately today it is possible to perform an experiment that shows the lines of force acting on two charged bodies.

In the following experiment the basic electric field lines can be observed by using a high-voltage DC supply, an insulating castor oil bath, and crushed felt particles (model railroad grass); refer to Figure D-11.

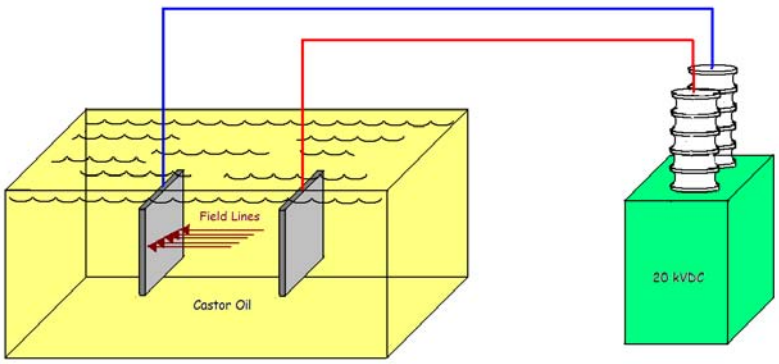

Figure D-11. Test setup to visualize electric field lines

In this experiment to determine how static electric field lines couple to the monopole antenna, one of the plates was replaced with the monopole antenna with the point of the antenna being at the position of the edge of the replaced plate and center of the remaining plate.

With 20,000 V_{DC} applied between the monopole antenna and the parallel plate, elapsed time photography was used to see the electric field lines; refer to Figure D-12. A high concentration of electric field lines exist at the point of the monopole antenna with electric field lines attaching along the length of each side of the antenna. The concentration of field lines at the point and along the length of the antenna indicates directivity and gain over that of a simple square plate that has been used for electric field sensors by others.

Figure D-12. Electric field lines between monopole antenna and a plate

These results add further support to the fact that the monopole antenna is highly directive; refer to Figure D-4. The results also explain why the monopole antenna is more efficient than the square plate sensor. The greater efficiency of the monopole antenna is attributed to the high concentration of field lines at the point of the antenna as discovered by Benjamin Franklin in his observation about points.

Appendix E

CIRCUIT DESIGN FOR THE HANDHELD DETECTOR

One important specification given by the utility sponsors was to have a simple single supply that is easily charged and has an extended operational time of 12 hours between charges. To accomplish this, a lithium-ion battery was used and the final circuits were developed around single-supply, rail-to-rail, surface-mount, low-energy-consumption integrated chips.

In the prototype, a simple single 9-volt supply source was step down to 5 V_{DC} and then a precision reference and op amp buffer were used to derive a dual-rail supply of ±2.5 V_{DC}. Refer to Figure E-1 for a schematic of the single-to-dual power supply circuit.

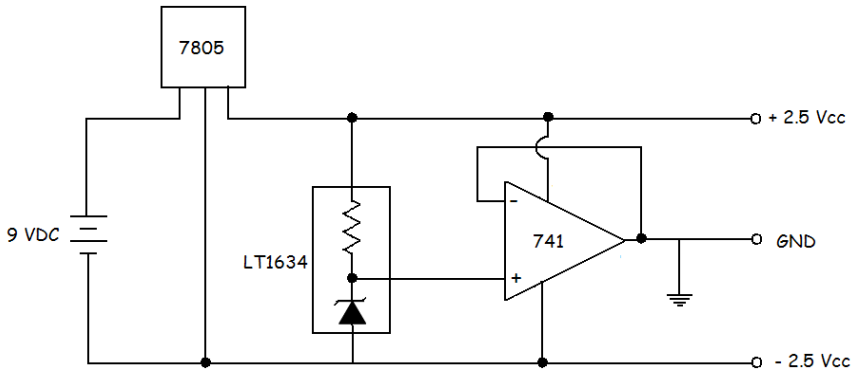

Figure E-1. Single-to-dual power supply circuit

The overall strategy of the analog handheld emissions detector is based on filters, detectors, derivatives, and voltage comparators.

Because the sensor head is based on the electric field and is intended to work in the high-impedance static field, an amplifier with a high-input impedance of at least

1 tera ohm (TΩ) was chosen for the input buffer. To obtain the high input impedance of the op amp, the circuit must be operated in the non-inverting configuration, refer to Figure E-2.

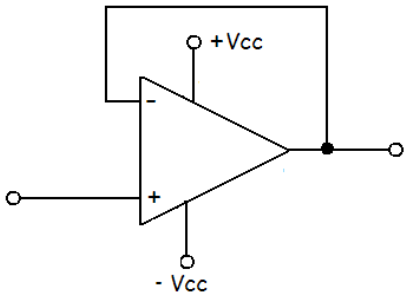

Figure E-2. High input impedance op amp

Other considerations that had to be considered were preserving the frequency bandwidth. Because of the high amplification required in the amplifier stages to detect a small electric field within a reasonable distance of 3 meters, the frequency bandwidth becomes limited in standard design practices. To detect an arcing source, the high-frequency content up to at least 40 kHz needs to be preserved.

Traditional instrumentation amplifiers have a typical open-loop bandwidth of 1 MHz, and in reality, with any gain, the amplifier usually does not perform beyond 10 kHz. A low-cost amplifier was identified that has a bandwidth of 3 MHz. This amplifier would allow the pass-band to exceed 30 kHz and allow for the use of only four stages of amplifications. Such an amplifier may have a total amplification of 40 dB (i.e., gain = 100); refer to Figure E-3.

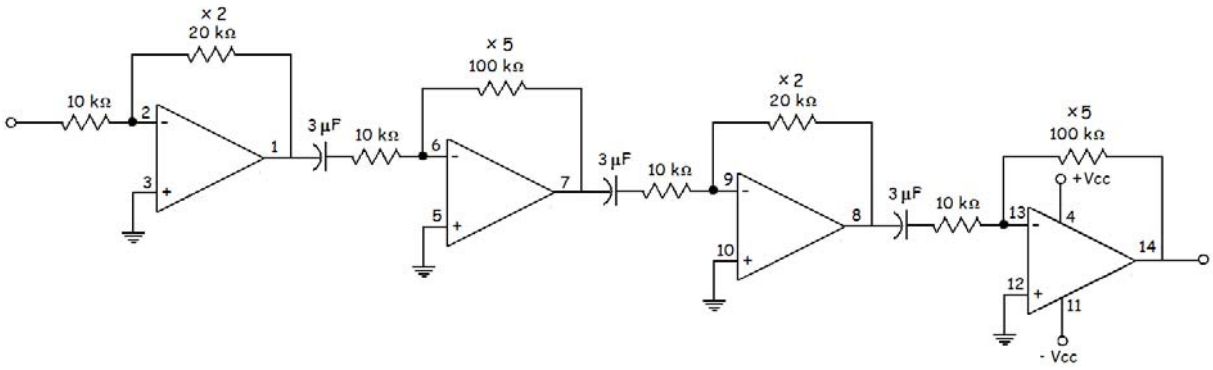

Figure E-3. Four-stage amplifier for a 40-dB amplification (i.e., gain = 100)

The frequency response of the amplifier stage may be seen in the bode plot in Figure E-4.

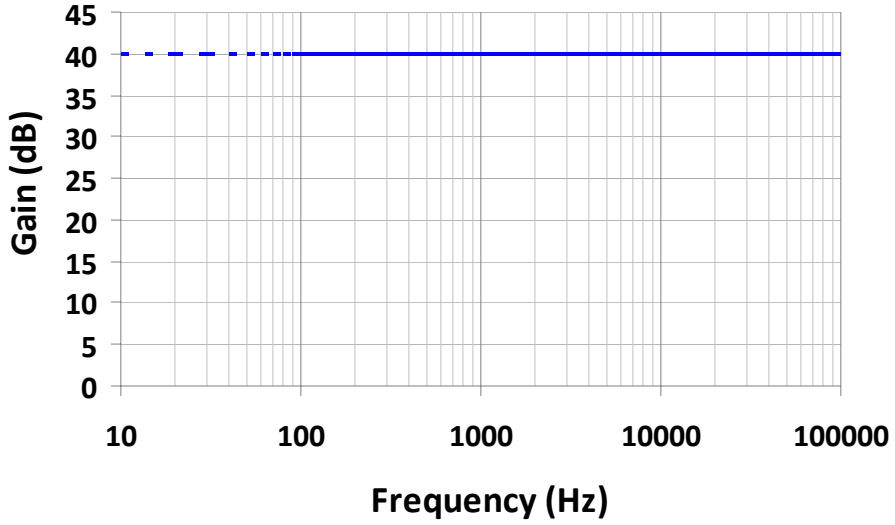

Figure E-4. Bode plot showing the frequency response of the amplifier stage

After the input buffer and amplifier stages, the signal is inverted and mixed with the fundamental frequency; see Figure E-5 and Figure E-6. Figure E-5 shows the circuitry just described. Figure E-6 shows the phase alignment on the left and the mixed and separated THD waveform output on the right. For test purposes, the third

harmonic is 50% of the fundamental and the resultant signal is the total harmonics minus the fundamental.

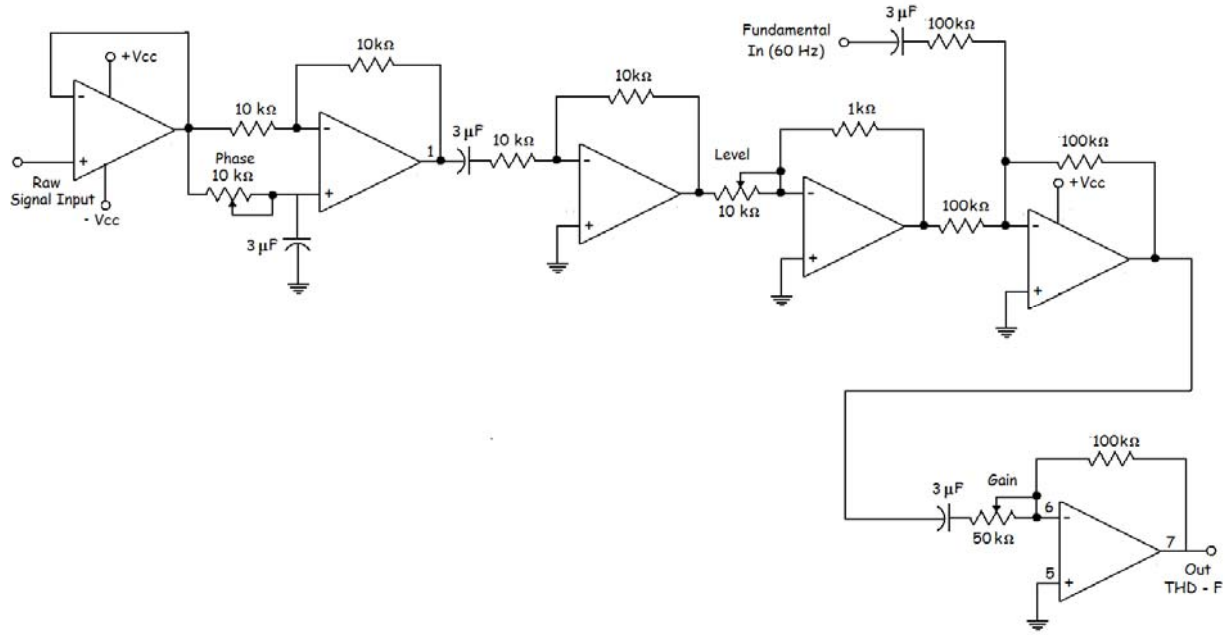

Figure E-5. Circuitry for THD separator

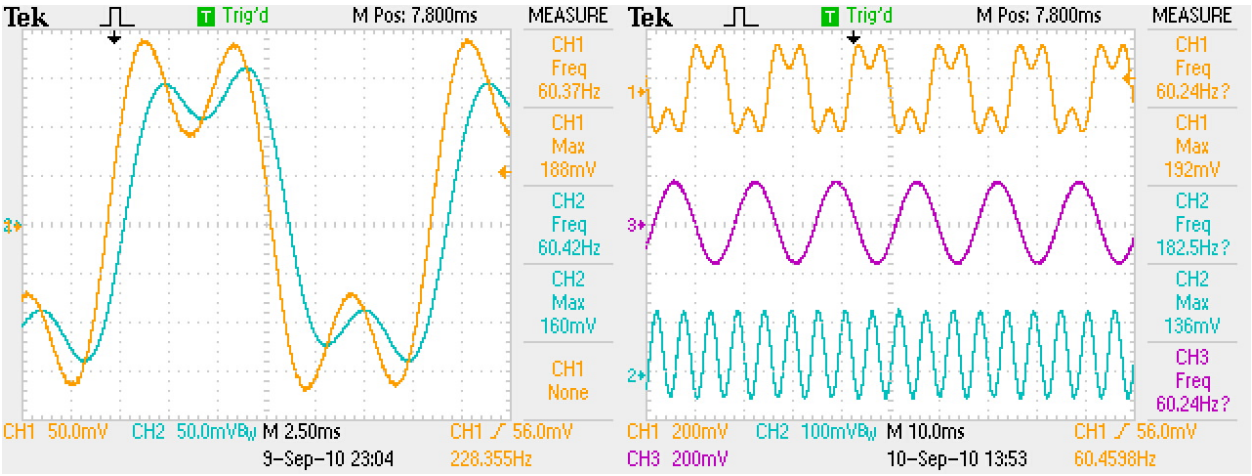

Figure E-6. THD separator waveforms

The fundamental 60 Hz is derived from the band-pass filter element within the programmable harmonic separator circuit; refer to Figure E-7.

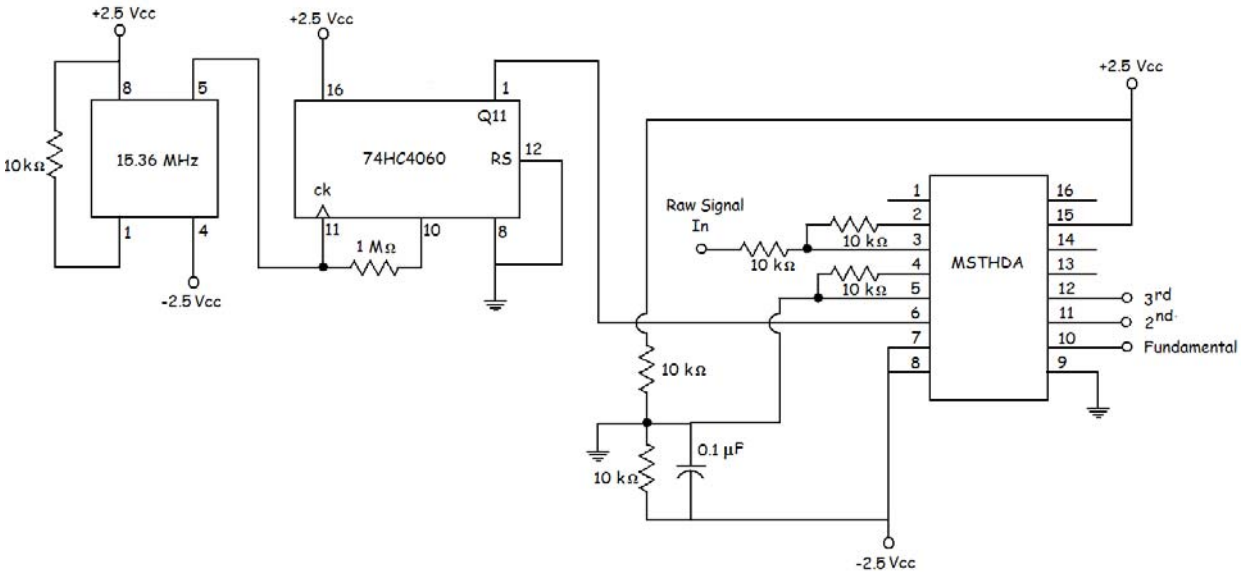

Figure E-7. Harmonic separator

Figure E-8 shows the waveforms separated by the THD circuit, where a mixed signal of 60, 120, and 180 Hz was used for test purposes.

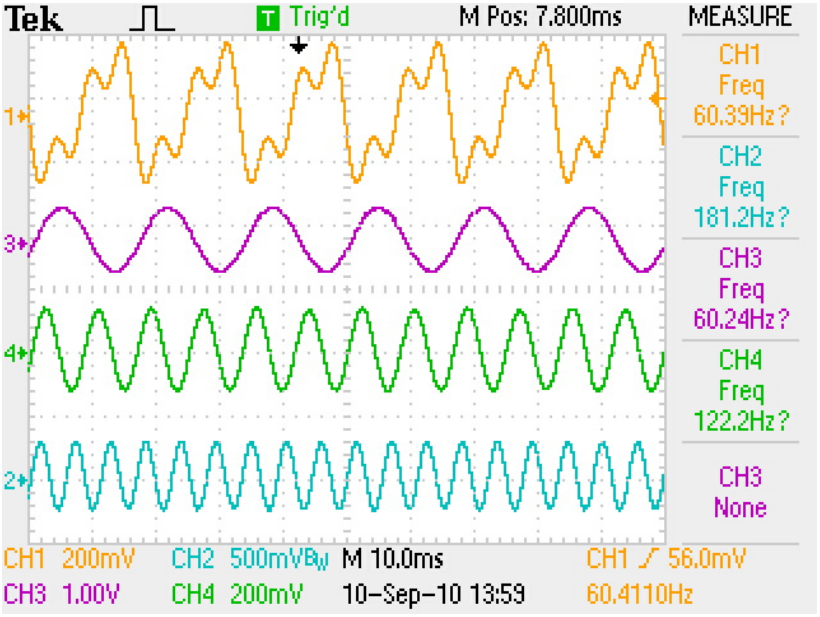

Figure E-8. Harmonic separator waveforms

The signals from the harmonic separator and fundamental canceller are passed through a precision rectifier to preserve both positive and negative peaks of the signal.

The use of the precision rectifier is required to preserve the signal quality before passing it to the detectors. Figure E-9 shows the circuitry for the precision rectifier. .

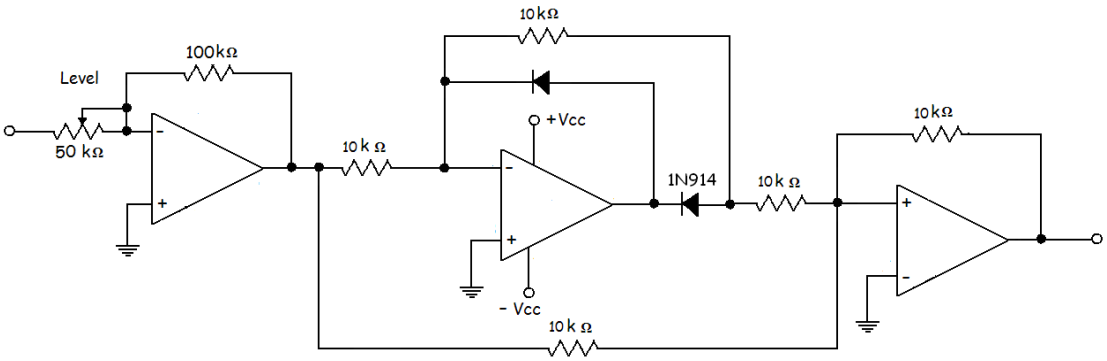

Figure E-9. Circuit for the precision rectifier

Figure E-10 shows the input waveform to the precision rectifier and the subsequent output waveform.

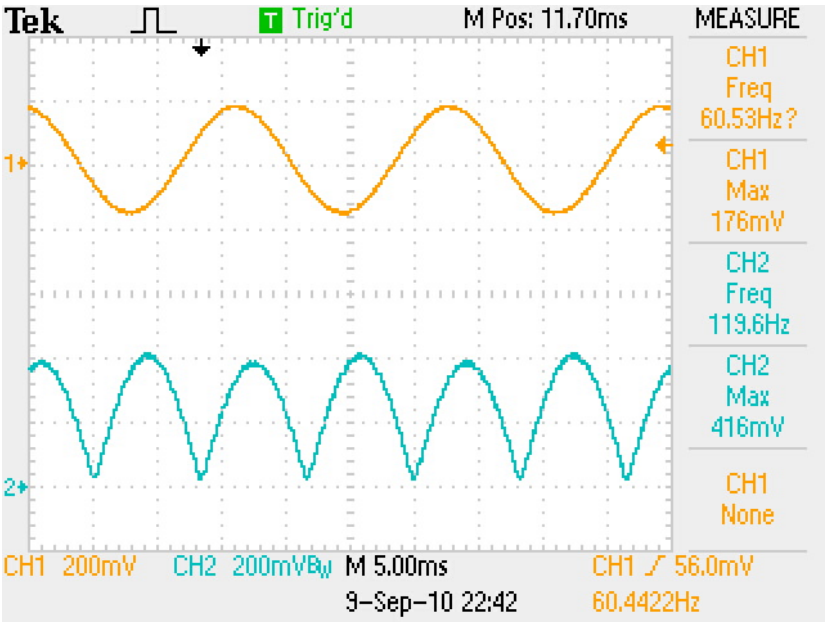

Figure E-10. Input and output waveforms for the precision rectifier

Once rectified, these signals are then passed though detector circuits and compared. If the harmonic signal is greater than 10% of the fundamental, then the

source of the energized object is a result of energized earth and not a result of direct wire contact. Refer to Figure E-11 for the detector and comparator circuit.

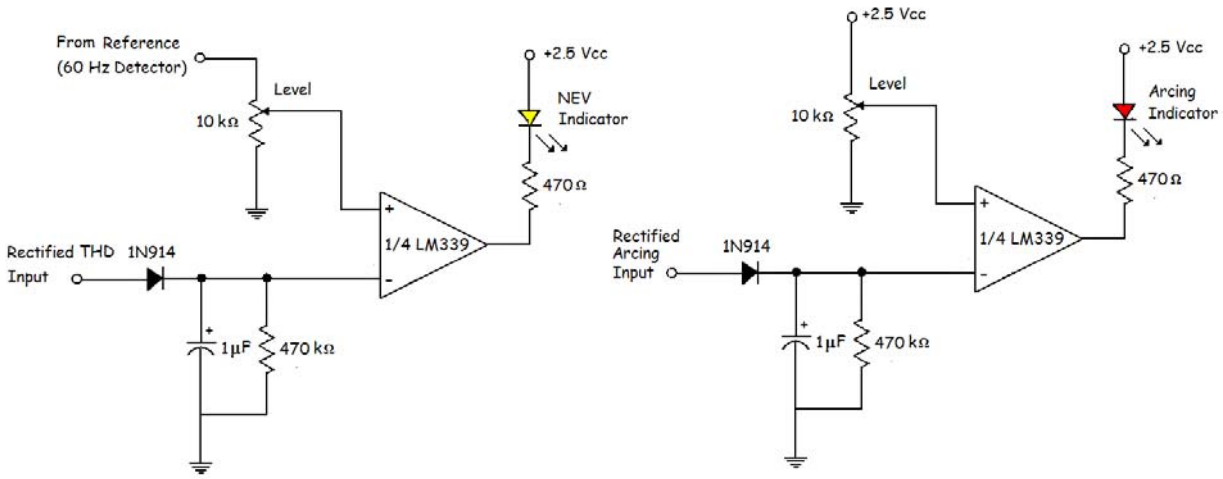

Figure E-11. Energized earth and arcing detectors and comparators

Figure E-12 shows the input and output waveforms of an energized earth signal passing through the detector and comparator circuit.

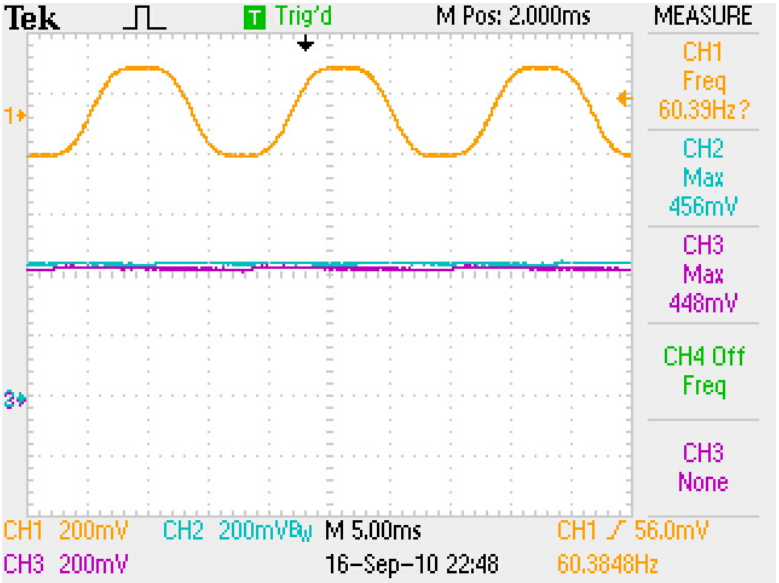

Figure E-12. Energized earth comparator waveforms

In a parallel effort by other researchers at EPRI, a key algorithm for detecting the presence of arcing is the use of the third derivative in a complex scheme of digital signal processing (DSP). This function has been simplified to reduce cost and limit the use a DSP chip.

An analog circuit has been developed for this project that reduces the complexity but is adequate for use in a handheld device for source identification. The derivative in essence acts as a high-pass filter.

As seen in Figure E-13, the arc detector is comprised of three derivative circuits with differing time constants to prevent saturation. The combination of the three circuits comprises the operation of a third derivative. (Phipps, 2010).

The resultant harmonic signal with the fundamental cancelled out is passed through a high-pass filter and two stages of derivatives for arc detection; refer to Figure E-13.

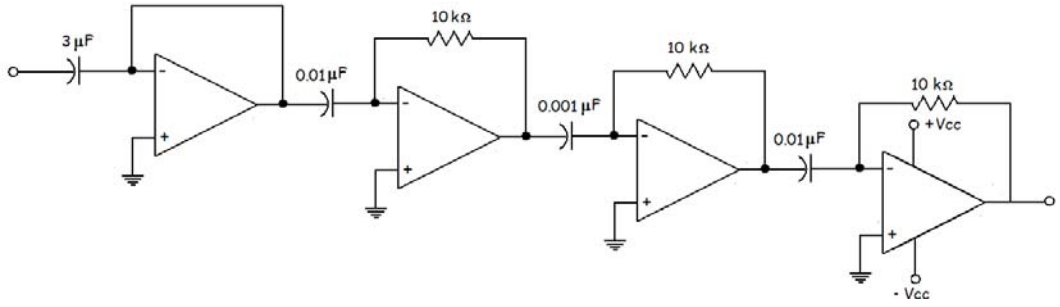

Figure E-13. Arcing-detection circuit, 3rd derivative

Afterwards, the signal is passed through a detector and fed directly to an LED indicator. In any condition where the LED is blinking, it is an indication that arcing is present. If the LED remains on constantly then a high-frequency source is identified

and it is a false positive. Figure E-14 shows the input and output waveforms for the arcing detection circuit.

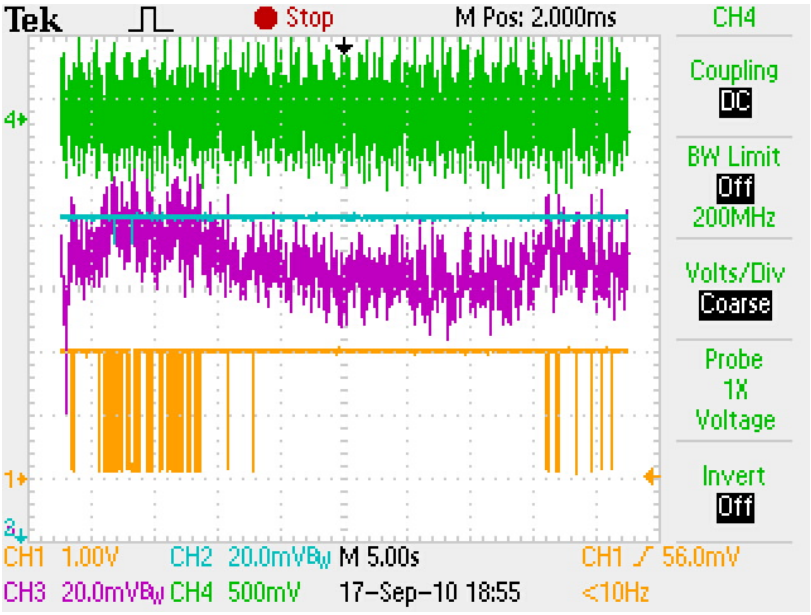

Figure E-14. Input and output waveforms for the arcing-detection circuit

The third harmonic signal from the harmonic distortion circuit is passed through a detector and is compared to the filtered fundamental signal from the same circuit. If the third harmonic is greater than the fundamental, the voltage source is a result from a magnetic field induction and there is a false positive.

The second harmonic signal from the harmonic distortion circuit is passed through a detector and is compared to the filtered third harmonic signal. If the second harmonic is greater than the third harmonic, the voltage source is a result from a nonlinear power supply such as a high voltage neon sign or other electronic light sources not fed directly from a 60 Hz source and is a false positive; refer to Figure E-15 and Figure E-16.

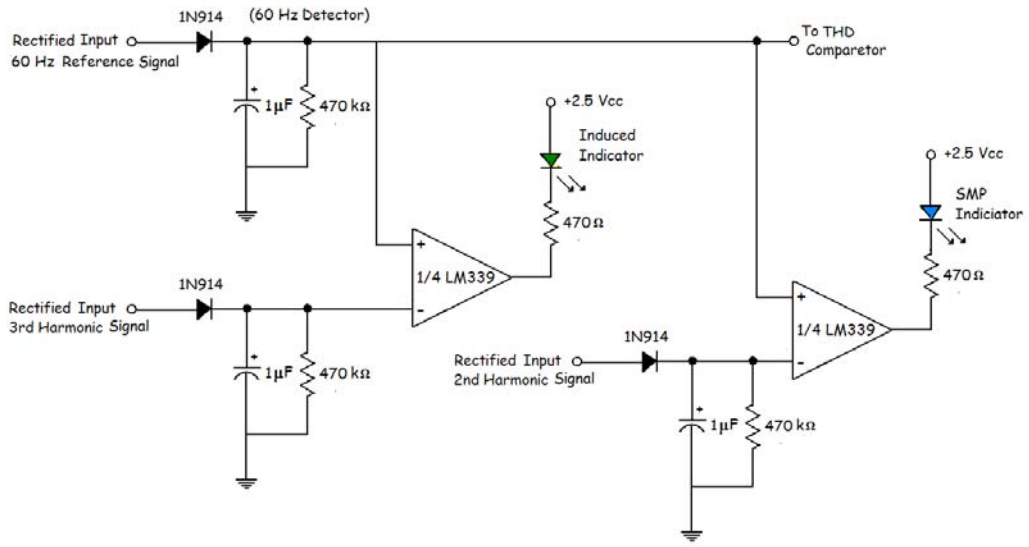

Figure E-15. Induction coupling and false positive detectors and comparators

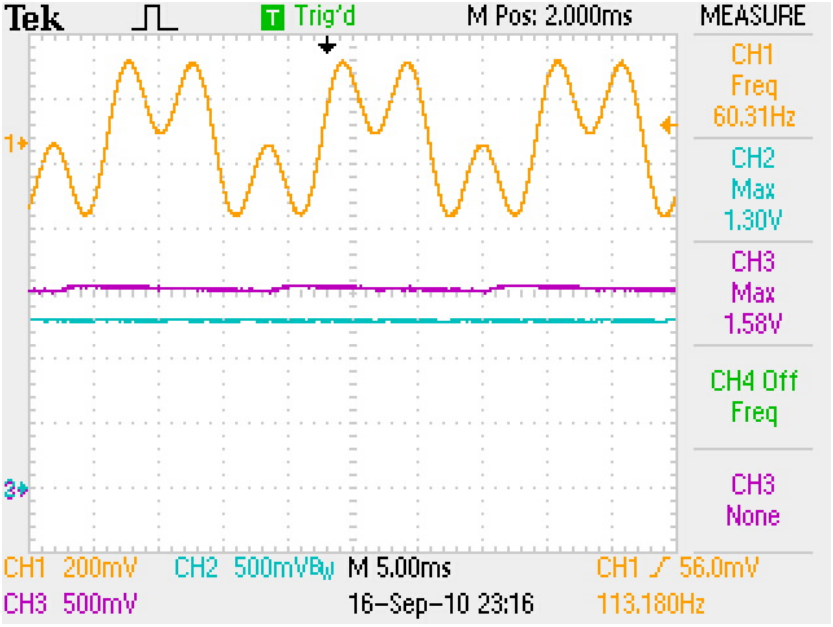

Figure E-16. Comparator waveforms

The filtered fundamental frequency eliminates false signals that may be associated with static discharge generated by walking.

LED Display Driver

The fundamental (60 Hz) signal is passed through an op amp that converts the voltage to an exponential function. It is then passed to the field strength detector circuit. Finally, it is passed to the LED display driver, an integrated circuit that senses DC voltage and activates one of ten LEDs depending on the field strength. Figure E-17 shows the number of LEDs activated versus field strength.

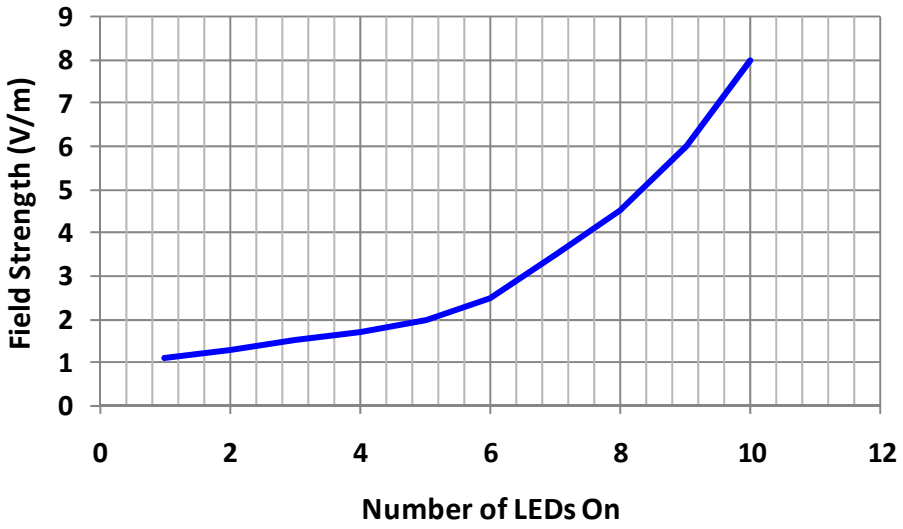

Figure E-17. Graph of the number of LEDs activated versus field strength

Appendix F

ADDITIONAL FUNCTIONS

Besides direct wiring contact, induction, and energized earth conditions, the handheld detector has been designed to detect two additional conditions: arcing, and false positives—created by an electronic source such as switch-mode power supplies for neon signs. An LED exists on the front panel of the handheld detector corresponding to each of these conditions.

Arcing

In general terms an arc begins with the breakdown of insulation. Then, an arc gap is formed (i.e., the distance between the insulation breakdown and ground). In the initial stages of the insulation breakdown, the current starts as sparks and may have magnitudes as small as a few milliamps. But as the current continues to ionize, the air molecules surrounding the arc gap and then full-blown arcing develops. The current continues to increase exponentially and the voltage rises to the point where intermittent arcing is sustained (Phipps, 2010).

Eventually, the arc will extinguish when the neutral return current becomes zero. Then, it will reoccur as the voltage again increases. During the initiation and extinguishing of the arc, sparks are generated and periods of high-frequency emissions are produced. Once the arc is established in the glow state, the high-frequency emissions drop off (Phipps, 2010).

In a parallel effort by other researchers at EPRI, a key algorithm for detecting the presence of arcing is the use the third derivative in a complex scheme of digital signal

processing (DSP). Differentiation is the mathematical method of computing the rate of change, where y is a function of x. This simple dependent relationship is shown in Equation F-1.

$$y = f(x) \quad \textbf{(F-1)}$$

While the rate of change is often used, it is the third derivative that has been determined to be effective in detecting arcs by current EPRI studies. The basic form of the third derivative is expressed in Equation F-2.

$$y = \frac{d^3}{dx^3} f(x) \quad \textbf{(F-2)}$$

Figure F-1 shows the recorded arc current generated in a manhole that is located 100 meters from an adjacent manhole and detected with a magnetic field sensor. As mentioned before, these data were recorded during a parallel EPRI research study. (Note: This study was independent of the research performed for this thesis.) (Phipps 2010).

In Figure F-1, the second trace from the top is the recorded magnetic field (also called H-Field) in the adjacent manhole while the arc was occurring. The third trace is the third derivative result from the processed magnetic field data. The third derivative captures the fast transients associated with the arc and the resulting trace corresponds to the arc current shown in the top trace.

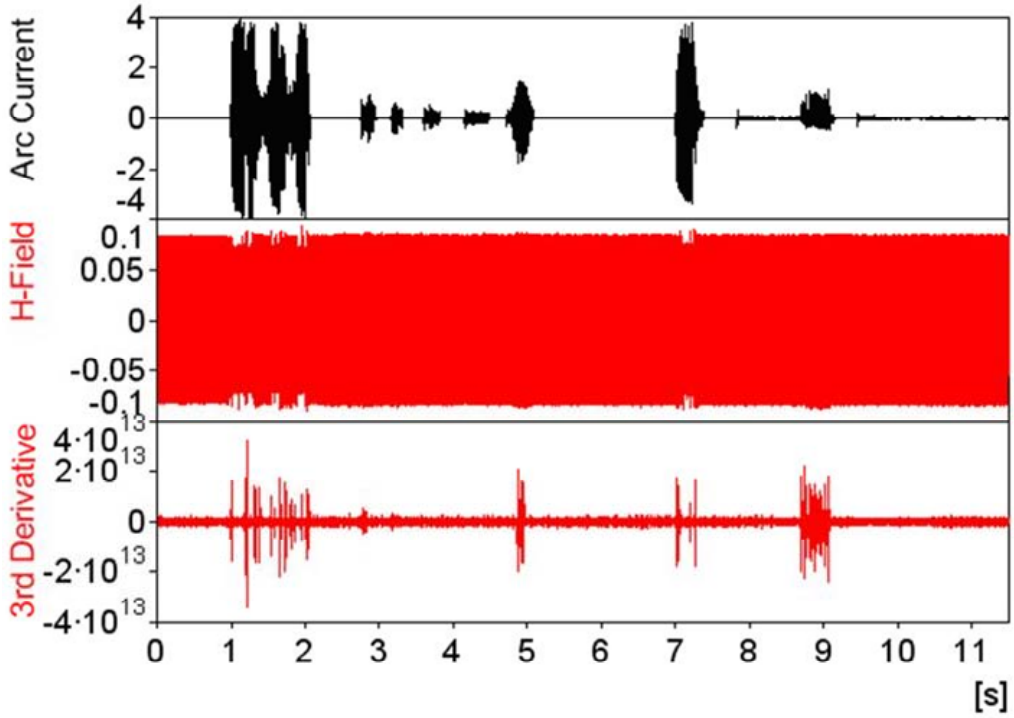

Figure F-1. Arc detection using third derivative of the raw signal (i.e., the arc current)

Switch-Mode Power Supplies

Switch-mode power supplies have one thing in common, they are full-wave rectified. The full-wave rectification results in a120 Hz ripple on the DC power supply rail that is then switched at a high frequency, typically at or above 27 kHz. This results in a modulated high frequency carrier of 27 kHz with an amplitude modulation of 120 Hz and other various intermodulation frequencies. The 120 Hz is dominant to all of the harmonics except for the fundamental frequency of 60 Hz; refer to Figure F-2.

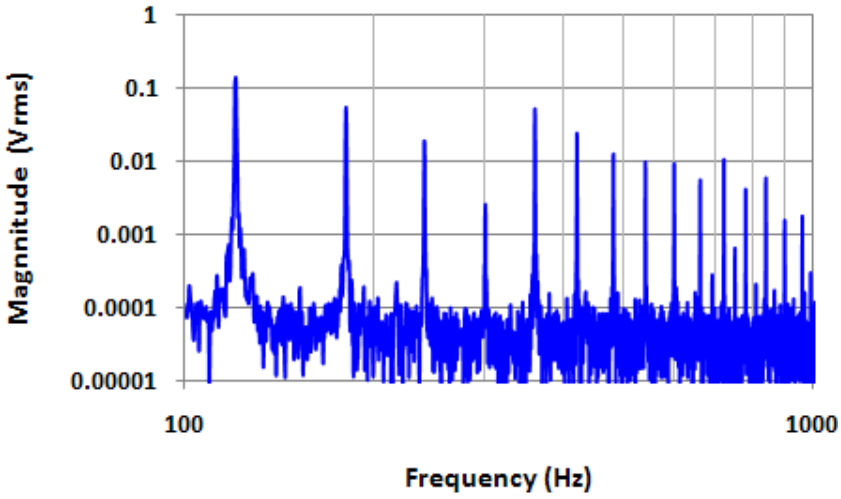

Figure F-2. Fast Fourier transform of electric field from neon sign (120 Hz greater than higher order harmonics)

If the 120 Hz modulation is not present in more advance power factor corrected power supplies, usually the even harmonics will be high because of nonsymmetry of the lamp waveform, refer to Figure F-3. When the waveform contains 60 Hz dominate frequency and with normal odd harmonics and virtually no even harmonics, the source is 60 Hz supplied from a ballast transformer and the signal cannot be distinguished from a contact source and results in a false positive.

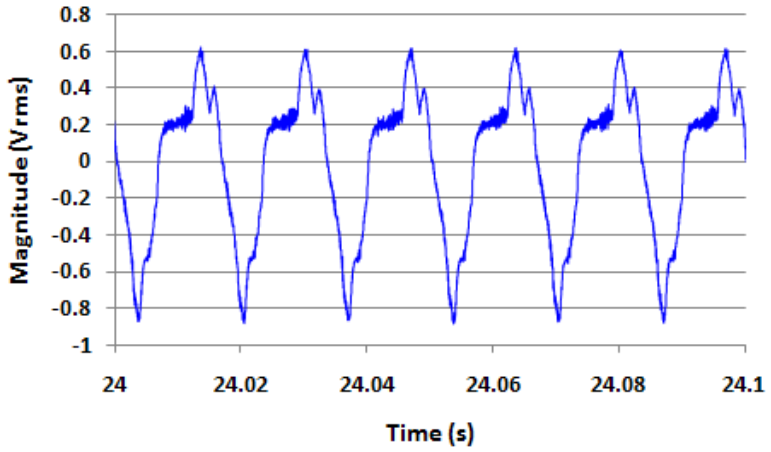

Figure F-3. Nonsymmetrical, electric-field waveform

VITA

KERMIT O. PHIPPS

Education:

MS in Technology, East Tennessee State University, Johnson City, Tennessee 2010

BS in Electronics Engineering Technology, East Tennessee State University, Johnson City, Tennessee 2008

AAS in Avionic Systems Technology, Community College of the Air Force, Maxwell AFB, Alabama 1989

Professional Experience:

Project Engineer/Scientist, Electric Power Research Institute, Knoxville, Tennessee, 1991 - Present

Publications:

Phipps, K. O., Keebler, P., and Arritt, R.F. (2009). “Real world ASD interference case study with modeled solutions,” IEEE EMC Symposium.

Phipps, K.O. and Keebler. P. (2006). “Applying an intelligent and automated emissions measurement to characterize the RF environment for supporting wireless technologies,” American Nuclear Society Conference.

Phipps, K.O. and Keebler P. (2001). “Update on the design and development of a portable radiated emissions measurement system for healthcare facilities,” IEEE EMC Symposium.

Phipps, K.O. and Geist, T. (1998) “100dB attenuation verification of EMI/RFI facility filters,” IEEE EMC Symposium.

Professional Activities:	Member Elect, Board of Directors of the IEEE EMC Society, 2010
	Senior Member of the IEEE EMC Society
	Secretary, IEEE EMC Society Technical Advisory Committee, 2009–present
	Standards Development Committee Member, IEEE EMC Society, 2009–present
	Chair, EMC Society TC-4 Committee, 2006–2009
	Secretary, EMC Society TC-4 Committee, 1998–2005
	IEEE 299.1 Working Group for 0.1 to 0.75 Meter Chambers, 2006–present
	Chairman, EEE 1560 Filter Measurement Standard. 1999–2005
Professional Recognition;	US Air Force Accommodation Medal, 1989.
	IEEE Power Engineering Society 2001 High Interest Paper Award.
	EPRI's Chauncey Award, Highest Award for Technical Contribution, 2009.
Pending Patents:	An improved method and apparatus for determining contact voltage sources.
	An improved method and portable apparatus to perform non-contact arc detection, recognition, and warning of same on electrical power lines by simultaneously evaluating characteristic waveform signatures in both the electric (E) and magnetic (H) fields.